FOI-R--1068--SE
December 2003
ISSN 1650-1942
Technical report

Martin Nilsson

Constitutive Model for Armox 500T and Armox 600T at Low and Medium Strain Rates

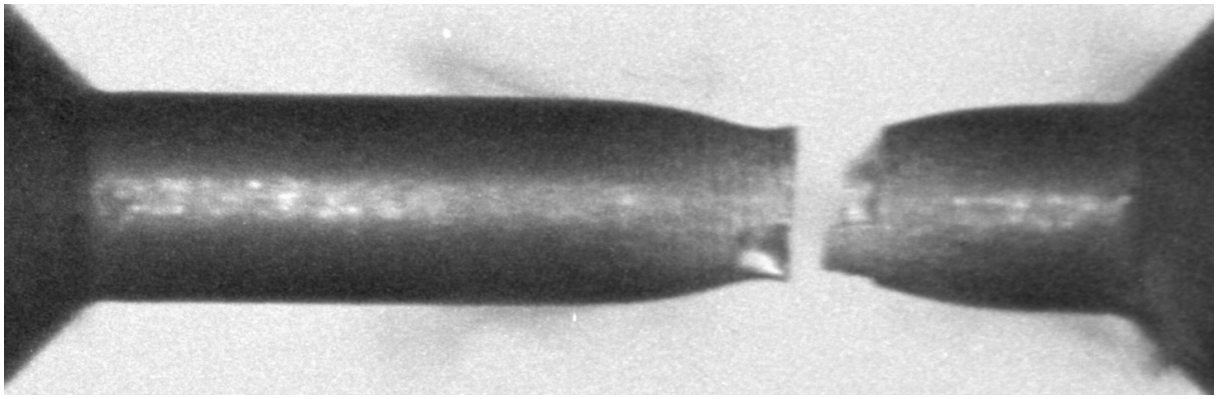

Weapons and Protection
SE-147 25 Tumba

SWEDISH DEFENCE RESEARCH AGENCY

Weapons and Protection
SE-147 25 Tumba

FOI-R--1068--SE

December 2003

ISSN 1650-1942

Technical report

Martin Nilsson

Constitutive Model for Armox 500T and Armox 600T at Low and Medium Strain Rates

This page is intentionally left blank

Sammanfattning

Höghållfasta pansarstål ger en hög nivå av skydd mot vapenverkan till en relativt låg kostnad och är ett intressant material för flyttbara skydd. Materialprovning är viktig både för att öka förståelsen om dynamiskt materialbeteende och för att kunna göra numeriska simuleringar av ballistiska förlopp. I den här rapporten presenteras försök utförda på Armox 500T och 600T, två höghållfasta pansarstål tillverkade av SSAB i Oxelösund, Sverige. Försöken har utförts vid olika töjningshastigheter och temperaturer och sedan har parametrarna i spänningsmodellen Johnson & Cook och två varianter av Johnson & Cook, föreslagna av Weerasooriya respektive Huang and Liang, och Zerilli & Armstrongs modell anpassats till experimentella data. För att kunna använda data insamlade efter att lokaliserad töjning uppträtt i provstavarna fotograferades provförloppet och spänning och töjning korrigerades enligt den av Bridgman föreslagna korrektionen. Försök utfördes för att undersöka isotropin hos stålen och för att fastställa kvasistatisk flytspänning och brottspänning. Experimentella data anpassades till de olika modellerna enligt olika rutiner. De olika rutinerna gav olika resultat och dessa jämfördes och kontrollerades för att upptäcka ofysikaliskt beteende. När resultaten jämfördes visade sig påtagliga skillnader mellan modeller och rutiner. Resultaten från försöken jämförs med data i litteraturen. Både försöken och litteraturdata visar att höghållfasta martensitiska pansarstål har lågt töjningshastighetshårdnande vid medelhöga töjningshastigheter, $\dot{\varepsilon} < 1000$ /s , jämfört med exempelvis kvävelegerat stål.

This page is intentionally left blank

Summary

High-hardness armour steels provide a high-performance protection at a relatively low cost and is an interesting material for movable shelters. Material testing is important both because of the need for understanding the dynamic material behaviour and as input in numerical simulations of ballistic events. In this report, experiments conducted on Armox 500T and 600T, two high hardness armour steels manufactured by SSAB in Oxelösund, Sweden. The experiments have been conducted at various strain rates and temperatures and the parameters in the strength models according to Johnson & Cook and variants of the Johnson & Cook proposed by Weerasooriya and Huang and Liang respectively, and Zerilli & Armstrong have been fitted to the experimental data. To be able to include data collected after necking, the neck was photographed during the test and stress and strain corrected according to Bridgman. Experiments were conducted to test the isotropy of the steel and quasi-static yield stress and rupture strength. The experimental data was fitted to the dynamic strength models following different fitting procedures. The different procedures give different results and these are compared and checked for unphysical behaviour. Plotting the results of all strength models and procedures show that the differences between different strength models and procedures are significant. The results from the experiments are to some extent compared with data found in the literature. Both the experiments and the literature shows that high-hardness martensitic armour steels have low strain-rate hardening at medium strain-rates, $\dot{\varepsilon} < 1000$ /s , compared to for example nitrogen alloyed steel.

This page is intentionally left blank

Contents

1 Introduction

Protection of personal and vital systems is always of high importance in military operations but especially so in peace-keeping or peace-enforcement operations. To provide protection, not only vehicles but also permanent or temporary structures, i.e. various field fortifications, need to provide a high degree of protection. High-hardness armour steels provide a high-performance protection at a relatively low cost and is an interesting material for all applications where the weight of the structure is of importance or when there is a need to de-assemble, move and re-assemble the structure.

Numeric simulations are an important tool in designing and evaluating fortifications but to conduct numerical simulations a thorough knowledge of the material properties is necessary. To conduct numerical simulations one needs a strength model, i.e. a mathematical model of the yield strength as a function of strain rate, strain and temperature, a fracture model, i.e. a mathematical model of the fracture behaviour, and an equation of state modelling the relation between pressure and volume.

In earlier work the properties of Rolled Homogenous Armour (RHA) [1] and High Nitrogen Steel (HNS) [2-4] have been published. In this report, experiments have been conducted in order to establish the parameters in the strength models according to Johnson & Cook [1] and variants of the Johnson & Cook strength model [5, 6] and to the Zerilli & Armstrong strength model [7] for Armox 500T and 600T, two high hardness armour steels manufactured by SSAB in Oxelösund, Sweden. To do this, the material needs to be tested at various strain rates. Low (quasi-static) strain rates can be achieved with the servo-hydraulic MTS system but for strain rates over approximately 10 /s other systems are needed. The most commonly used method to reach medium strain rates ($10^2/\mathrm{s} < \dot{\varepsilon} < 10^4/\mathrm{s}$) is the Hopkinson bar [8-16]. Even higher strain rates at controlled experimental conditions are achievable using either Taylor impact ($10^4/\mathrm{s} < \dot{\varepsilon} < 10^5/\mathrm{s}$) or plate impact ($\dot{\varepsilon} > 10^5/\mathrm{s}$). The materials also need to be tested at temperatures well above room temperature to simulate the effects of large strains at high strain rates under adiabatic conditions. The high temperature testing is achieved using an inductive heater, but this heater can only be used together with the MTS system at quasi-static strain rates.

The results are to some extent compared with results found in the literature. Lach et al. [17] carried out mechanical testing on a martensitic armour steel, with the German designation 1.6568 and a hardness of 500 HV30 and Nahme and Lach [18] studied the French Mars armour steels.

2 Materials

Armox 500T and Armox 600T are two examples of modern armour steels manufactured by SSAB[1] in Oxelösund, Sweden. The number in the product designation is the approximate hardness measured as Brinell grades. The engineering properties, as supplied by the producer, are found in Table 1. $R_{p0.2}$ is the yield strength at 0.2% plastic deformation and for high strength steels this is usually considered to be the initial yield strength. R_m is the highest load a rod of the metal can carry, using engineering strength, i.e. load divided by initial cross sectional area. A_5 is the elongation after fracture measured over five diameters. *HBW* is Brinell hardness measured using a tungsten carbide indentor. Charpy-V is a method of measuring the impact strength at low temperatures using a notched sample.

Table 1. Mechanical properties[1].

	Armox 500T	**Armox 600T**	**Standard**
$R_{p0.2}$ / MPa	1250 (minimum)	1500 (typical)	
R_m / MPa	1450-1750	2000 (typical)	
A_5 / %	8 (minimum)	7 (typical)	
Hardness/ *HBW*	480-540	570-640	EN ISO 6506-1
Charpy-V at -40°C/ J	20 (minimum)	12 (minimum)	EN 10 045-1

No tests were performed to validate nominal elastic and thermal properties and the chemical composition found in Table 2 and Table 3.

[1] Data sheet from SSAB, <www.ssabox.com>

Table 2. Nominal material properties.

	Armox 500T	**Armox 600T**
Elastic modulus, E / GPa	207	207
Specific heat capacity, c_p / J/kgK	450	450
Density, ρ / kg/m^3	7850	7850
Melting temperature, T_m / K	1800	1800

Table 3. Chemical composition according to the manufacturer[2].

	Armox 500T	**Armox 600T**
C max %	0.32	0.47
Si %	0.1-0.4	0.1-0.4
Mn max %	1.2	1.0
P max %	0.015	0.010
S max %	0.010	0.005
Cr max %	1.0	1.5
Ni max %	1.9	3.0
Mo max %	0.7	0.7
B max %	0.005	0.005

[2] Data sheet from SSAB, <www.ssabox.com>

3 Methods

3.1 Specimen design

The samples were cut from the middle of a 10 mm thick plate. All specimens had the same design with the exception of the gauge length (*L*) and the length of the threaded section (*G*), Figure 1. Dimensions of samples used according to Table 4.

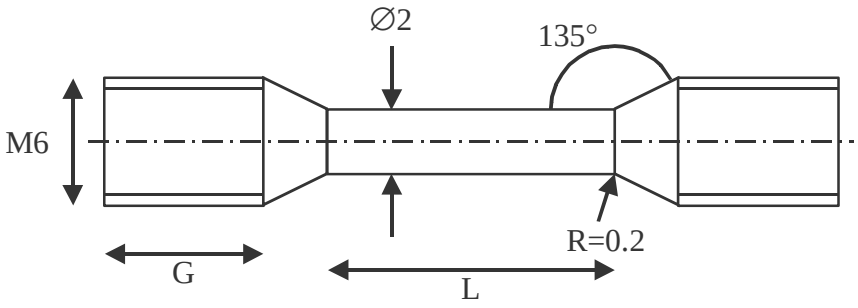

Figure 1. Specimen design.

In Figure 2 a photography of a sample is shown. The sample is died black to improve the contrast when photographing the experiments, see section 3.2.2.

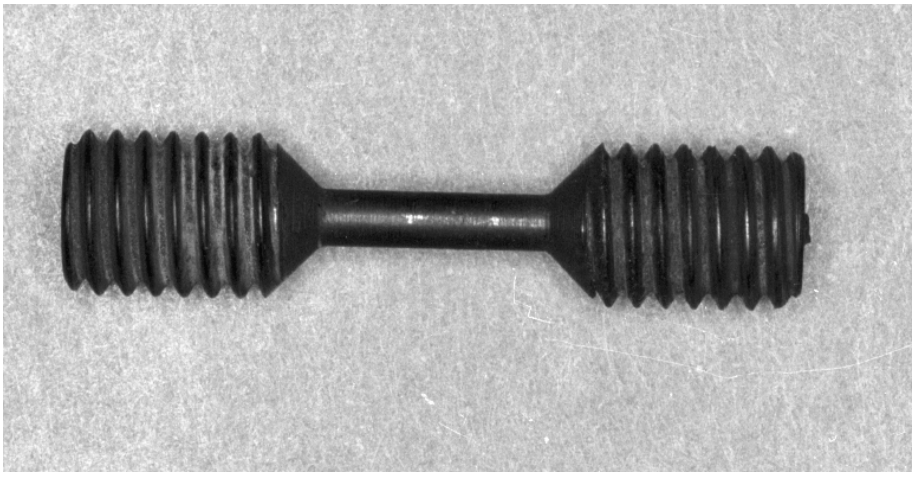

Figure 2. Specimen.

Table 4. Specimen dimensions.

Direction	L/mm	G/mm	Tests
Normal to rolling direction	8	7	$\dot{e} \approx 0.001$ /s at 20 °C $\dot{e} \approx 1$ /s at 20 °C $\dot{e} \approx 400$ /s at 20 °C
Normal to rolling direction	8	10	$\dot{e} \approx 1$ /s at 300 °C $\dot{e} \approx 1$ /s at 400 °C $\dot{e} \approx 1$ /s at 500 °C
Normal to rolling direction	4	7	$\dot{e} \approx 800$ /s at 20 °C
Parallel to rolling direction	8	7	$\dot{e} \approx 0.001$ /s at 20 °C $\dot{e} \approx 1$ /s at 20 °C

In Table 4, $\dot{e}$ is the engineering strain rate, i.e. related to the undeformed sample. A compilation of the experiments is found in Appendix A.

3.1.1 Length to diameter ratio

In a study by Staab and Gilat [14] it is shown that the length to diameter ratio of a tensile Hopkinson specimen has to be greater than 1.6 to avoid boundary effects.

Table 5. Allowed length/diameter ratio [14].

Diameter/mm	Smallest allowable length/mm
1.50	2.40
2.00	3.20
3.00	4.80

In this study the diameter of the samples were 2 mm and had a smallest length of 4 mm and as can be seen from Table 4, the length-to-diameter ratio was kept above 1.6.

3.2 Low strain rate tests

At low strain rates ($\dot{\varepsilon} \leq 1$ /s) a servo-hydraulic MTS tensile testing machine was used. The tests were performed at a constant displacement velocity.

The use of an inductive heater coupled to an IR-camera allowed for tests at elevated temperatures, Figure 3.

Figure 3. Close-up of the inductive heater and the IR-camera.

3.2.1 Stresses and strains before necking

The treatment of the experimental raw data measured with the servo hydraulic system and the Hopkinson apparatus were done in a similar way as in an earlier work by Skoglund [19].

- Necking was assumed to occur at maximum stress and hence, data points after necking were ignored, Figure 4.
- The data were corrected for play and compliance and since the constitutive equations require knowledge of the plastic deformation only, the elastic part of the specimen deformation was subtracted and the plastic strain was calculated according to (1), as shown in Figure 4, Figure 5 and Figure 6.

$$\varepsilon_{plastic} = \varepsilon_{app} - \frac{\sigma_{nom}}{E_{app}} - \varepsilon_0 - 0.002 \qquad \textbf{(1)}$$

- In (1) ε_{app} is the apparent strain as measured in the experiments, σ_{nom} is the nominal stress as measured in the experiments and E_{app} is the apparent elastic modulus including elastic deformations in both specimen and testing machine. E_{app} is derived from the slope of the engineering stress-engineering strain curve between 30% and 60% of the maximum engineering stress using a least square fit. ε_0 is the intercept of the fitted line at zero stress, i.e. the apparent elastic modulus, and the abscissa. The factor 0.002 (0.2%) is the strain setoff usually used to define the yield point in high strength metals.

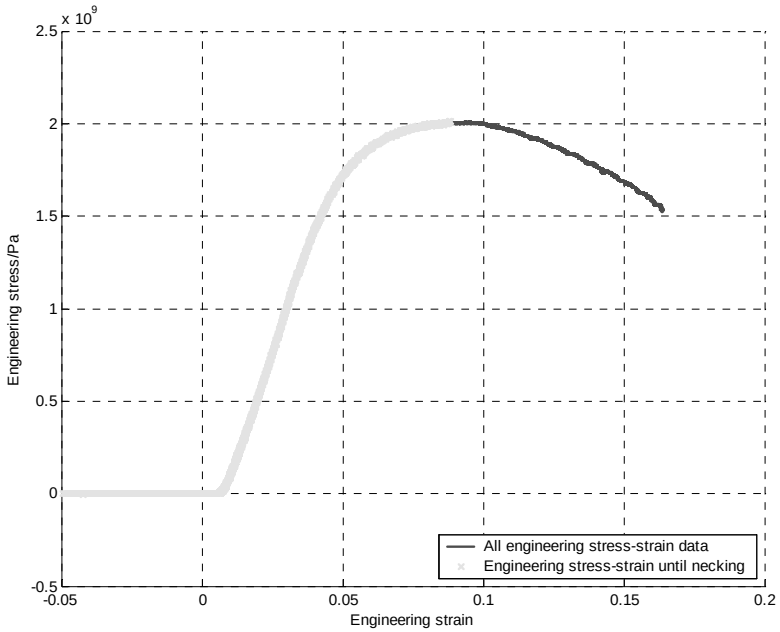

Figure 4. Extraction of data until necking (sample A6_05). Note that the strain is not corrected for play.

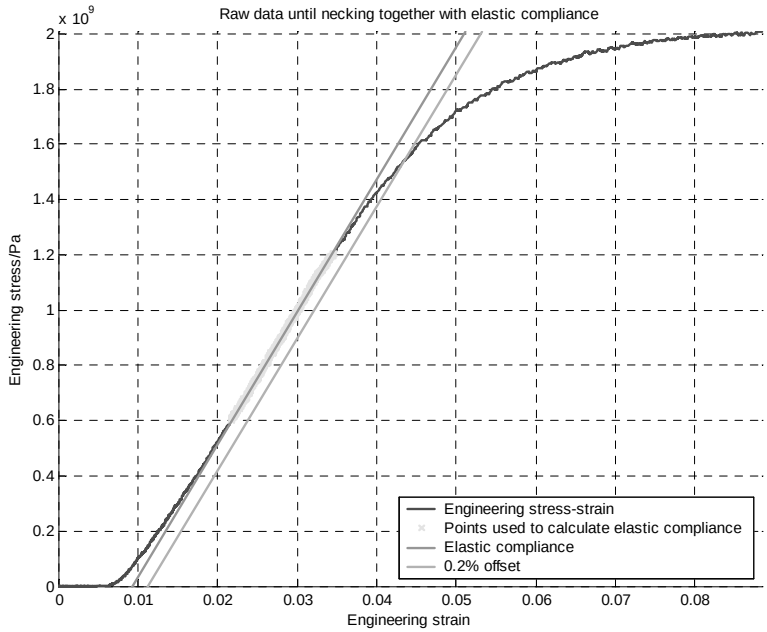

Figure 5. Extraction of the plastic strain and stress (sample A6_05). Note that the strain is not corrected for play.

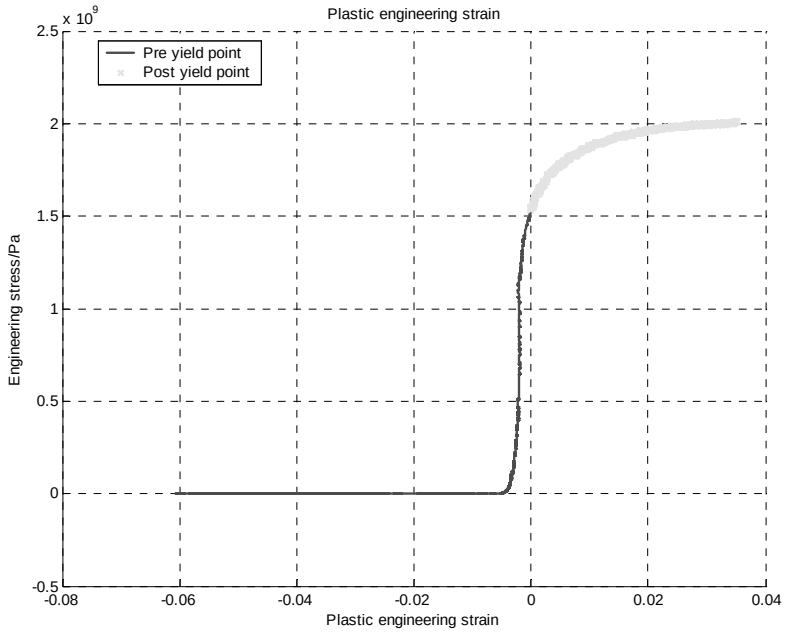

Figure 6. Plastic engineering strain and stress (sample A6_05).

Engineering stresses and strains were recalculated as true stresses and strains, (2) and (3).

$$\varepsilon_{true} = \ln\left(1+\varepsilon_{eng}\right) \quad \textbf{(2)}$$

$$\sigma_{true} = \sigma_{eng}\left(1+\varepsilon_{eng}\right) \quad \textbf{(3)}$$

The data volume was reduced so that a maximum of 200 data points from each experiment are used in further curve fitting.

Because of a high sampling rate, 1 kS/s even at low strain rates, the engineering strain rate had a high noise level at low strain rates, Figure 7. This signal was discarded and the time derivative of a polynomial fitted to the true strain was used instead. In Figure 7 both the time derivative of the true strain rate, the solid line, and some of the pints from the engineering strain rate are plotted.

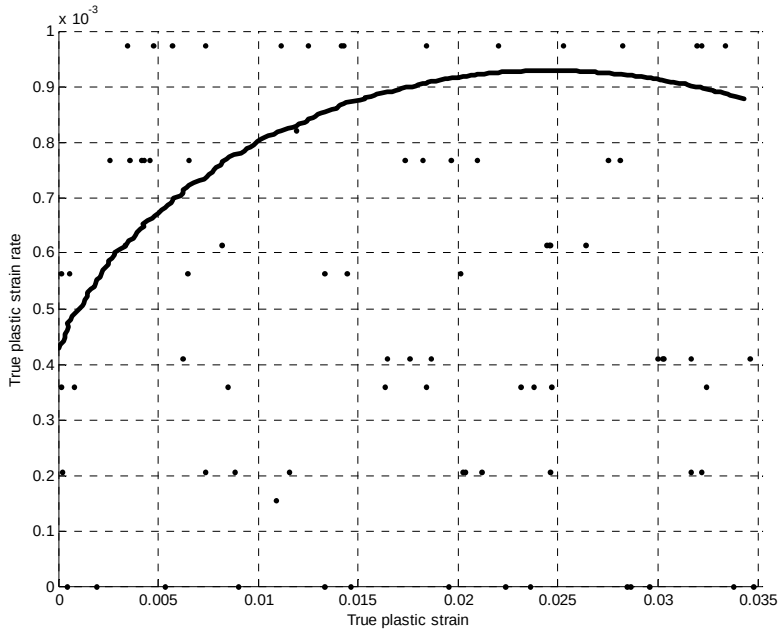

Figure 7. True plastic strain rate from quasi-static tensile test (sample A6_05).

3.2.2 Stress and strain after necking

To be able to include data collected after necking, the development of the neck was photographed at 3 second intervals and stress and strain corrected according to Bridgman [20].

First, the strain can be calculated using the constancy of volume during plastic deformation,

$$\frac{dl}{l} = -\frac{dA}{A} \Rightarrow \tag{4}$$

$$\varepsilon = \ln\frac{A_0}{A} = \ln\frac{\frac{\pi d_0^2}{4}}{\frac{\pi d^2}{4}} = 2\ln\frac{d_0}{d} \tag{5}$$

where l is the sample length, A_0 and A is the initial and the apparent cross-sectional area of the sample respectively and d_0 and d is the initial and the apparent diameter of the sample respectively.

Secondly, the stress corrected for necking is calculated using the relation [20],

$$\sigma = \frac{F}{\pi\frac{D^2}{4}}\frac{1}{\left(1+\frac{4R}{D}\right)\ln\left(1+\frac{D}{4R}\right)}, \tag{6}$$

where F is the axial force, D is the diameter of the cross-section at the neck and R is the radius of curvature of the neck, Figure 8.

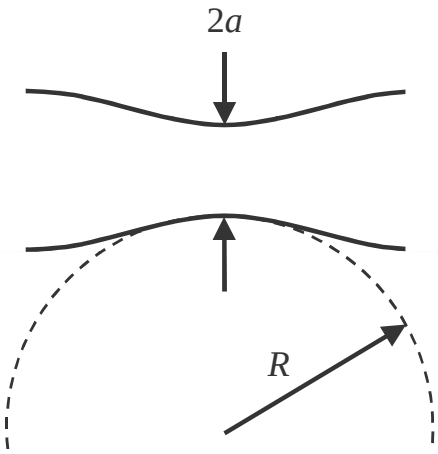

Figure 8. Necked specimen.

The set-up for photographing the samples during testing is shown in Figure 9. The camera used was an ordinary Nikon 35 mm camera. A picture was taken approximately every 3 seconds. The signal from diode II, i.e. a time record of the flash, was stored together with time, force and displacement in the MTS recorder.

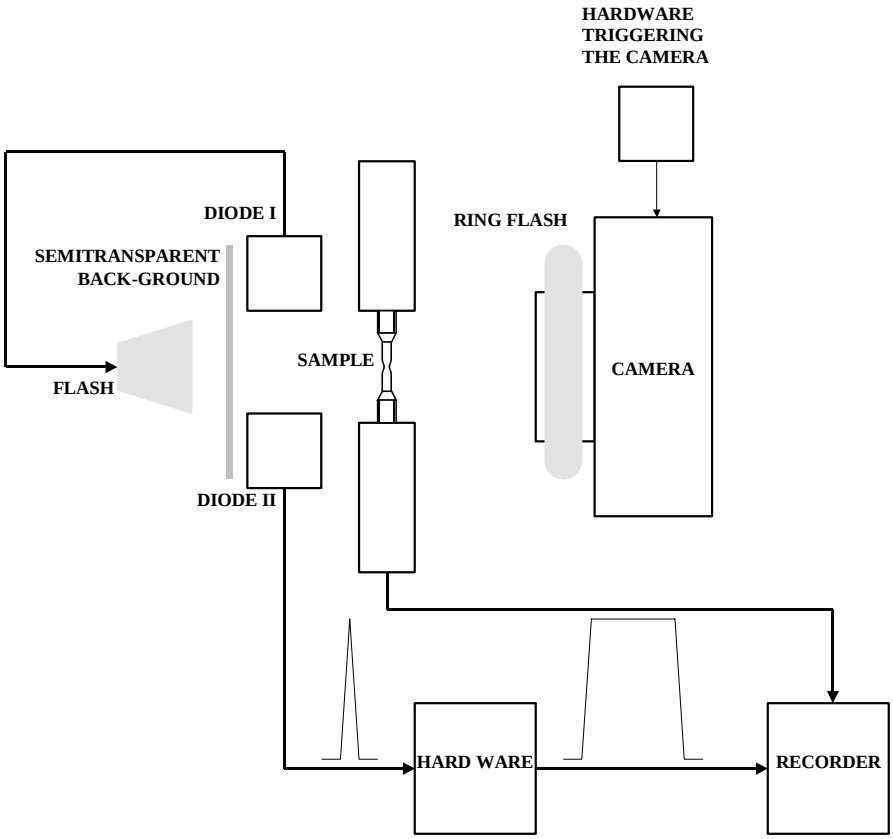

Figure 9. Set-up with servo-hydraulic testing machine and camera equipment.

The photos were scanned at highest possible resolution, imported into Matlab and by calculating the gradient of the pixel values the edge was detected. The coordinates of the edge were used to calculate the diameter and radius of curvature, Figure 8.

3.3 Medium strain rate tests

At medium strain rates ($100 < \dot{\varepsilon} < 1000$/s) a single bar tensile Hopkinson apparatus [13] was used. The tensile force was generated with a pendulum. The experiments and the evaluation of the signals were done in accordance with Svensson [13].

The experiments at medium strain rates were performed at room temperature. The temperature rise in these experiments was due to heating from plastic deformation.

Figure 10. Single bar tensile Hopkinson apparatus [13].

3.3.1 Adiabatic heating during tensile tests

Based on the results from Skoglund [4] deformation at strain rates of $1\,/\mathrm{s}$ and higher are considered adiabatic. The heating is calculated using

$$\Delta T = \frac{\varphi}{\rho c_p}\int_0^{\varepsilon}\sigma(\varepsilon)d\varepsilon\,. \qquad \textbf{(7)}$$

Values of ρ and c_p are found in Table 2. The ratio of work transformed to heat, φ, was set to 0.9 thereby implying that 10% of the work is stored in the material as defects [21].

3.3.2 Force equilibrium during dynamic tensile tests

In the following section an attempt is made to estimate at what strain force equilibrium prevails. A reasonable assumption is that three plastic stress wave reverberations are required for stress equilibrium in a split Hopkinson bar sample.

The wave speed is given by

$$c_{plastic} = \sqrt{\frac{\partial\sigma/\partial\varepsilon}{\rho}}. \quad \textbf{(8)}$$

A common way to describe the yield stress as a function of strain is

$$\sigma_Y = A + B\varepsilon^n. \quad \textbf{(9)}$$

The strain derivative of (9) is

$$\frac{\partial\sigma_Y}{\partial\varepsilon} = nB\varepsilon^{n-1}. \quad \textbf{(10)}$$

Combining (8) and (10) leads to

$$c_{plastic} = \sqrt{\frac{nB\varepsilon^{n-1}}{\rho}} = \sqrt{\frac{nB}{\rho}}\varepsilon^{\left(\frac{n-1}{2}\right)}. \quad \textbf{(11)}$$

If the strain rate is assumed to be constant, the strain at time t after yielding is given by

$$\varepsilon = \dot{\varepsilon}_0 t \quad \textbf{(12)}$$

and the plastic wave speed at time t by

$$c_{plastic} = \sqrt{\frac{nB}{\rho}}\left(\dot{\varepsilon}_0 t\right)^{\left(\frac{n-1}{2}\right)}. \quad \textbf{(13)}$$

The plastic wave speed in (13) will render unphysical values at small strains or times if $n<1$,

$$\dot{\varepsilon}_0 t \to 0 \Rightarrow c_{plastic} \to \infty, \quad \textbf{(14)}$$

and when plotting it versus strain or time it is rewritten

$$c_{plastic} = \min\left[\sqrt{\frac{E}{\rho}},\quad \sqrt{\frac{nB}{\rho}}\left(\dot{\varepsilon}_0 t\right)^{\left(\frac{n-1}{2}\right)}\right]. \quad \textbf{(15)}$$

As an approximation, assuming uniform strain in the sample but keeping in mind that it is not, the distance travelled by the plastic wave is the time integral of (13),

$$S = \int_0^t c_{plastic}\,dt = \int_0^t \sqrt{\frac{nB}{\rho}}\left(\dot{\varepsilon}_0 t\right)^{\left(\frac{n-1}{2}\right)} dt = \frac{2}{(n+1)\dot{\varepsilon}_0}\sqrt{\frac{nB}{\rho}}\left(\dot{\varepsilon}_0 t\right)^{\left(\frac{n+1}{2}\right)}. \quad \textbf{(16)}$$

Solving (16) for the time needed for m reverberations,

$$S = m2l_s, \quad \textbf{(17)}$$

where l_s is the sample length, gives

$$t = \frac{1}{\dot{\varepsilon}_0}\exp\left(-\frac{1}{n+1}\ln\left(\frac{nB}{m\rho l_s^2\dot{\varepsilon}_0^2(n+1)^2}\right)\right). \quad \textbf{(18)}$$

Combining (12) and (18) gives the strain at m reverberations,

$$\varepsilon = \exp\left(-\frac{1}{n+1}\ln\left(\frac{nB}{m\rho l_s^2\dot{\varepsilon}_0^2(n+1)^2}\right)\right) \quad \textbf{(19)}$$

In section 5.4.4 the parameters B and n are extracted for various data sets. Using the parameters derived with the MTS data set, Table 6, i.e. the best fit to small strains, and solving (19) for 3 reverberations gives the plastic wave speed according to Figure 11 and strains-to-force-equilibrium according to Figure 12 and Figure 13 respectively. As will be shown later, the values in Table 6 are not valid for large strains.

Table 6. Parameters used for plastic stress wave calculation.

	B **/GPa**	n
Armox 500T	2.37	0.505
Armox 600T	3.95	0.552

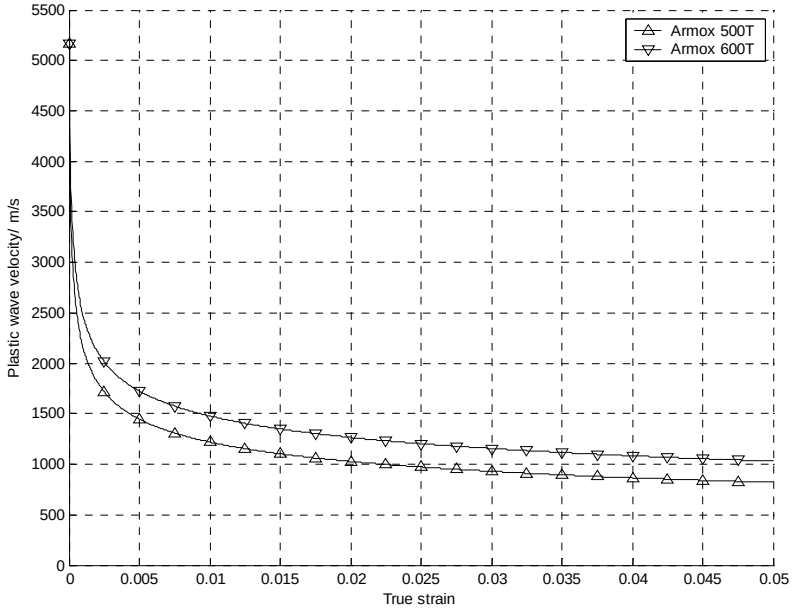

Figure 11. Plastic wave speed as a function of strain.

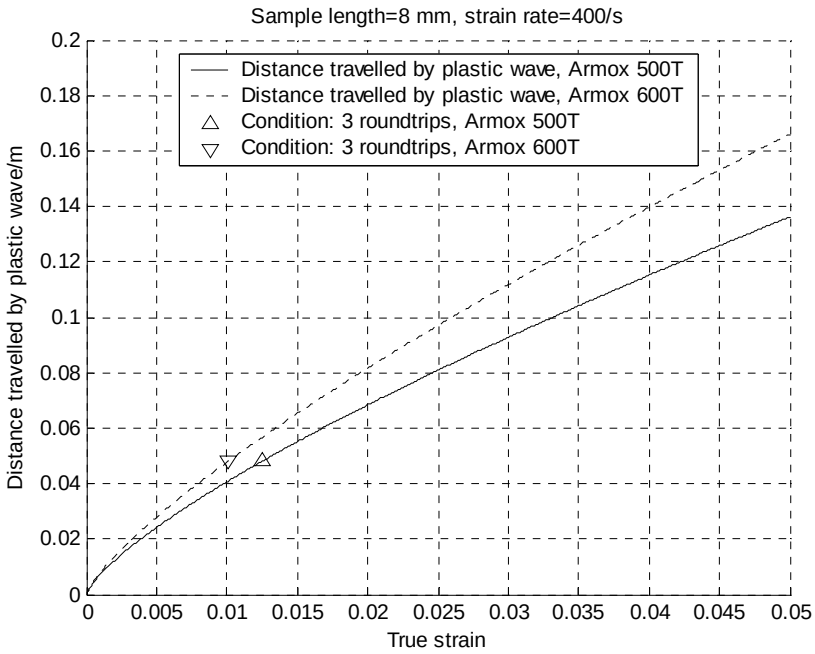

Figure 12. Strain needed to reach stress equilibrium, sample length 8 mm.

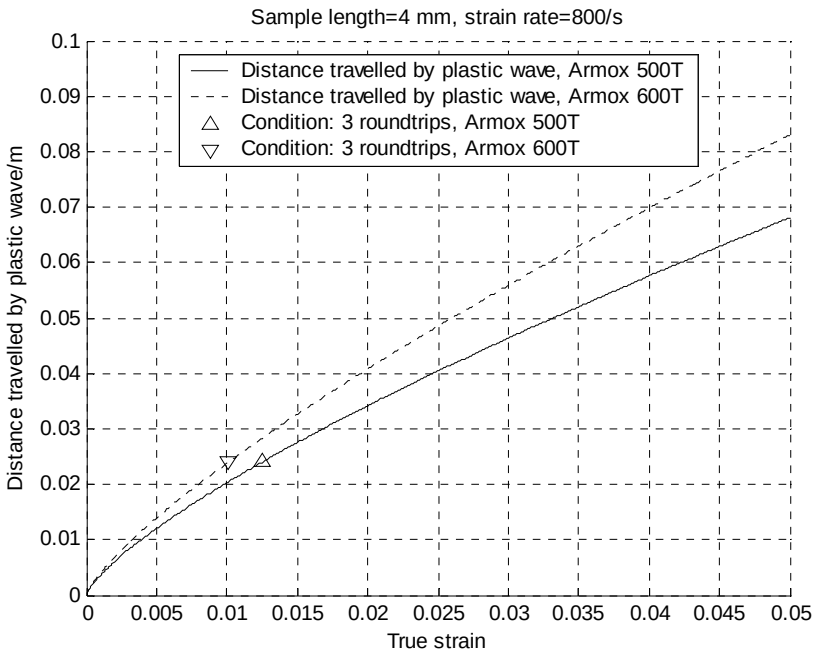

Figure 13. Strain needed to reach stress equilibrium, sample length 4 mm.

A conservative conclusion is that stress values at strains lower than about 1,5% should be discarded.

4 Material models

4.1 Quasi-static material models

4.1.1 Power law

The power law model (20) is very simple and gives a good approximation of stress for large, quasi-static strains. The strain in the model is the total strain, elastic and plastic.

$$\sigma_Y = K\varepsilon^n \tag{20}$$

In (20), K and n are constants.

4.1.2 Elastic-plastic linear hardening

In an elastic-plastic linear hardening material the yield stress is assumed to be the minimum of two functions of strain,

$$\sigma_Y = \min([E\varepsilon, \quad P\varepsilon + k]). \tag{21}$$

The strain in the model is the total strain, elastic and plastic. In (21), E is the elastic modulus and P and k are constants.

4.2 Dynamic Material models

4.2.1 Johnson & Cook and variants

The Johnson & Cook strength model [1] has for some time been the workhorse of numerical modelling. It is basically an empirical expression of the dependence of the yield strength on strain, strain rate and temperature. The dependencies are not coupled to each other. The abbreviation is JC. The yield stress is given by

$$\sigma_Y = \left(A + B\varepsilon^n \right)\left(1 + C \ln \frac{\dot{\varepsilon}}{\dot{\varepsilon}_0} \right)\left(1 - \left(\frac{T - T_0}{T_{melt} - T_0} \right)^m \right), \tag{22}$$

where A, B, C, m and n are constants and $\dot{\varepsilon}_0$ is a reference strain rate set to 1 /s, T_0 is the reference temperature, in this study set to 293 K and T_{melt} is the melting temperature of the metal, in this study set to 1800 K.

An important thing to observe is that the strain rate term in the original JC implementation, (23), and subsequence implementations in hydrocodes such as for example Autodyn, strain rates lower than 1 /s is set to 1 /s, i.e. deformations at strain rates lower than 1 /s uses the strain hardening term at 1 /s. But, as will be shown later in section 5.5, Armox 500T and Armox 600T show low strain rate hardening effects at strain rates lower than 1000 /s and the discussion about strain hardening in section 5.2 is thus valid.

$$\left(1+C\max\left[0,\quad \ln\frac{\dot{\varepsilon}}{\dot{\varepsilon}_0}\right]\right) \tag{23}$$

During the years following the publication of the Johnson & Cook strength model many variants have been published. Here, two variants with different temperature dependencies are used.

Weerasooriya [5] used a variation of the Johnson & Cook model where the temperature dependence is modified. The abbreviation is JCW. The yield stress in this model is given by

$$\sigma_Y = \left(A+B\varepsilon^n\right)\left(1+C\ln\frac{\dot{\varepsilon}}{\dot{\varepsilon}_0}\right)\left(1-\left(\frac{T-T_0}{T_{melt}-T_0}\right)\right)^m . \tag{24}$$

Huang and Liang [6] suggested a third temperature dependence adding two parameters, D and E. The abbreviation is HL. The yield stress in this model is given by

$$\sigma_Y = \left(A+B\varepsilon^n\right)\left(1+C\ln\frac{\dot{\varepsilon}}{\dot{\varepsilon}_0}\right)\left(D-E\left(\frac{T-T_0}{T_{melt}-T_0}\right)^m\right). \tag{25}$$

4.2.2 Zerilli & Armstrong

Zerilli and Armstrong [7] suggested the model since then known as the Zerilli & Armstrong strength model. The model has more of a physical background since it couples the dependence between temperature and strain rate and has different formulations depending on crystal type, body centred cubical (BCC) or face centred cubical (FCC). Since Armox steel is BCC, equation (26) is the BCC formulation. The abbreviation is ZA. The yield stress is given by

$$\sigma_Y = \sigma_G + C_1\exp\left(-C_3T + C_4T\ln\frac{\dot{\varepsilon}}{\dot{\varepsilon}_0}\right) + C_5\varepsilon^n . \tag{26}$$

In (26) σ_G, C_1, C_3, C_4, C_5 and n are constants to be determined for each material.

5 Results

5.1 Isotropy

To test the isotropy of the steels, tensile tests were conducted with samples cut both parallel and normal to the rolling direction, Figure 14.

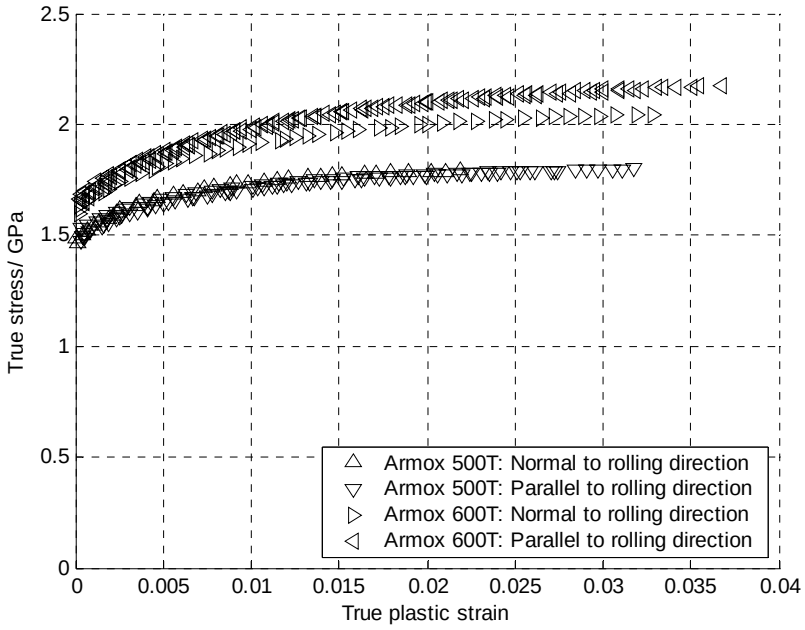

Figure 14. Samples taken normal and parallel to the rolling direction. Strain rate 1 /s and room temperature.

The tests on Armox 500T show no anisotropy but with Armox 600T there is an indication that the strain hardening is slightly higher parallel to the rolling direction. Only experimental data normal to the rolling direction were used in the fitting process.

5.2 Quasi-static yield stress

Using stress-strain measurements at the lowest strain rate, engineering strain rate of 0.001 /s, the yield stress was calculated as the mean value of the yield stress of three experiments, A5_05, A5_06, A5_11 and A6_05, A6_06, A6_11, respectively, Table 7.

Table 7. Quasi-static yield stress.

	$R_{p0.2}$/GPa
Armox 500T	1.47
Armox 600T	1.58

The results are in accordance with data supplied form the manufacturer, Table 1.

5.3 Quasi-static rupture strength

Using stress-strain measurements at the lowest strain rate, engineering strain rate of 0.001 /s, rupture stress was calculated as the mean value of the rupture stress of three experiments, A5_05, A5_06, A5_11 and A6_05, A6_06, A6_11, respectively, Table 8.

Table 8. Quasi-static rupture stress.

	R_m/GPa
Armox 500T	1.77
Armox 600T	2.04

The results are in accordance with data supplied form the manufacturer, Table 1.

5.4 Strain hardening

Using force and displacement data collected with the MTS system at an engineering strain rate of 0.001 /s gave the stress-strain curves in Figure 15. Combining force and time measurements from the MTS system, with data derived from photographing the sample, calculating the strain using (5) and the stress correction (6) according to Bridgman [20] gave the results in Figure 16. The data derived with the Bridgman correction method was adjusted for elastic strains, i.e. reduced with the elastic portion.

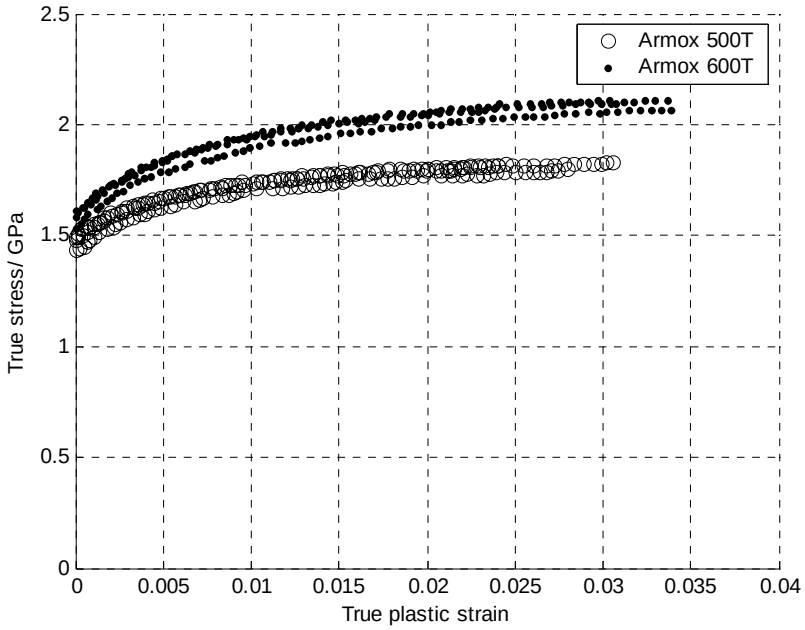

Figure 15. Samples taken normal to the rolling direction. Strain rate 0,001 /s and room temperature.

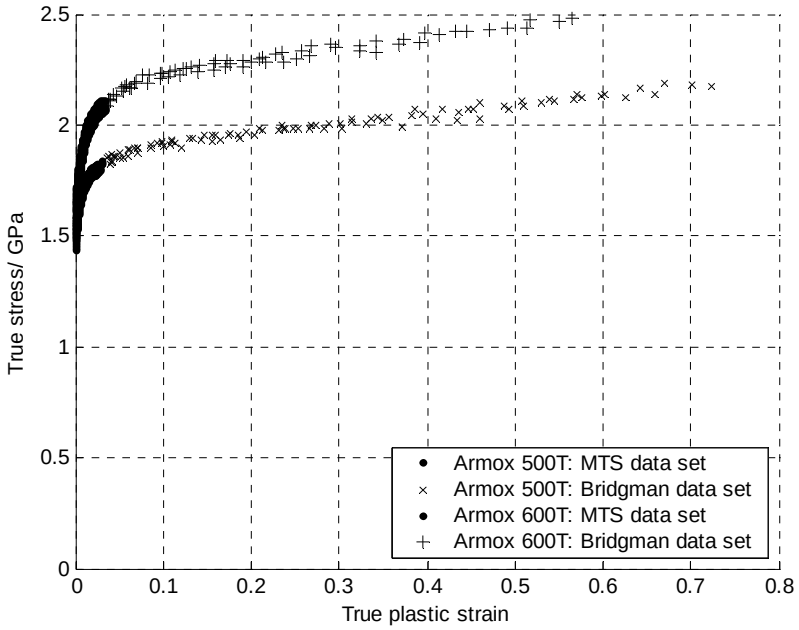

Figure 16. Samples taken normal to the rolling direction. Strain rate 0,001 /s and room temperature.

The data derived using the Bridgman correction described above was compared with the results from a simplified method by Le Roy et al. [22]. Le Roy experimentally established the ratio between a, the sample radius at the neck and R, the radius of curvature of the neck,

Figure 8, as a function of true strain and the true strain at necking, i.e. true strain at ultimate tensile strength ε_{UTS},

$$\frac{a}{R} = k\left(\varepsilon - \varepsilon_{UTS}\right). \quad \textbf{(27)}$$

Furthermore Le Roy et al [22] derived that $k = 1.11$ for steel, turning (27) into

$$\frac{a}{R} = 1.11\left(\varepsilon - \varepsilon_{UTS}\right). \quad \textbf{(28)}$$

In Figure 17 the stress values calculated using the measured values from the photographs and stresses calculated using the method proposed by Le Roy et al. [22], i.e. equation (28), are compared showing good agreement.

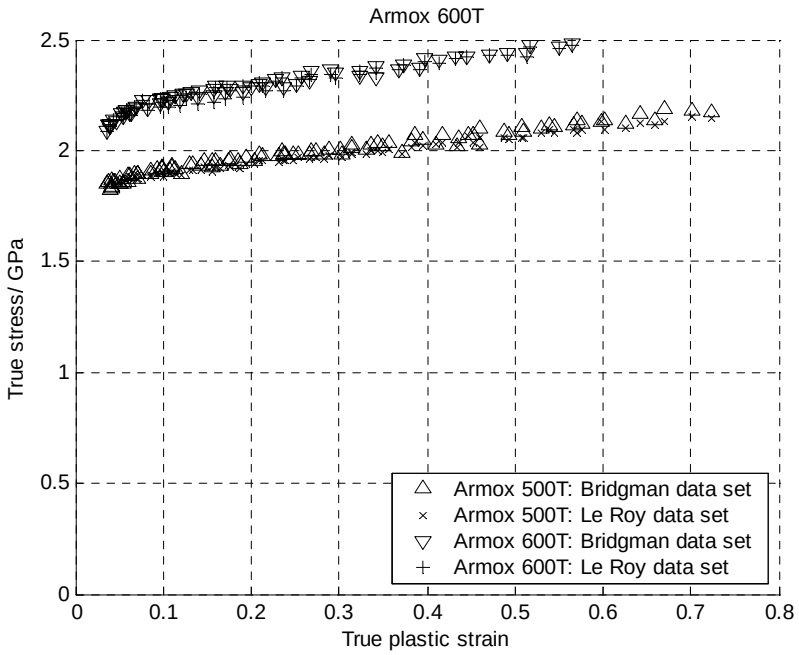

Figure 17. Comparison between the Bridgman and Le Roy methods.

5.4.1 Power law

The power law model was fitted with the Bridgman data set unadjusted for elastic strains. Equation (20) is rewritten into

$$\sigma_Y = K\varepsilon^n \Rightarrow \ln\left(\sigma_Y\right) = \ln K + n\ln\varepsilon\,. \quad \textbf{(29)}$$

This problem can be solved using the least square method.

Table 9. Power law parameters.

	K /GPa	n
Armox 500T	2.16	0.0544
Armox 600T	2.52	0.0569

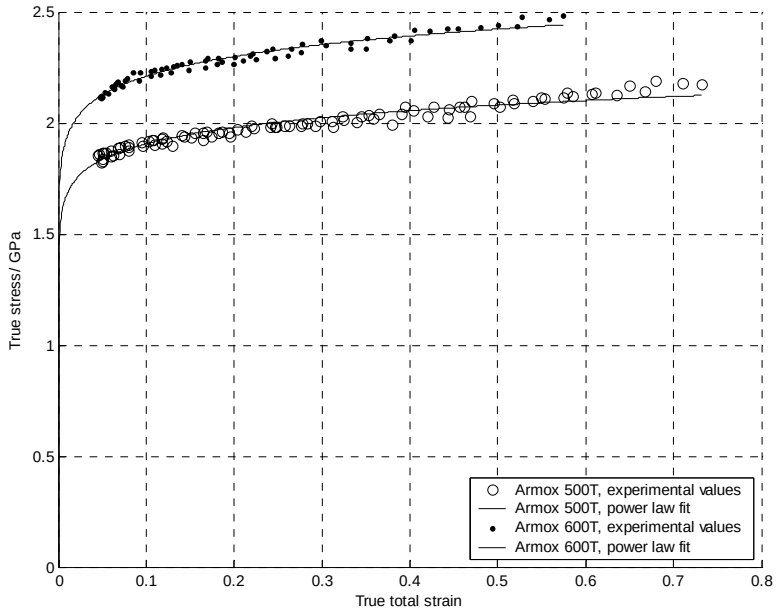

Figure 18. Data set and power law fit.

As seen in Figure 18, the power-law model gave good agreement with the experimental data.

5.4.2 Elastic-plastic linear hardening

In an elastic-plastic linear hardening material the yield stress is assumed to be the minimum of two functions of strain,

$$\sigma_Y = \min\left(\left[E\varepsilon, \quad P\varepsilon + k\right]\right), \tag{30}$$

where E is the elastic modulus and given by Table 2 as 207 GPa. P is the plastic modulus and k is a stress offset, both derived by fitting a straight line to the Bridgman data set unadjusted for elastic strains,

$$\sigma_Y = P\varepsilon + k\,. \tag{31}$$

This problem can be solved using least square method.

Table 10. Elastic-plastic linear hardening parameters.

	E /GPa	P /GPa	k /GPa
Armox 500T	207	0.467	1.85
Armox 600T	207	0.632	2.14

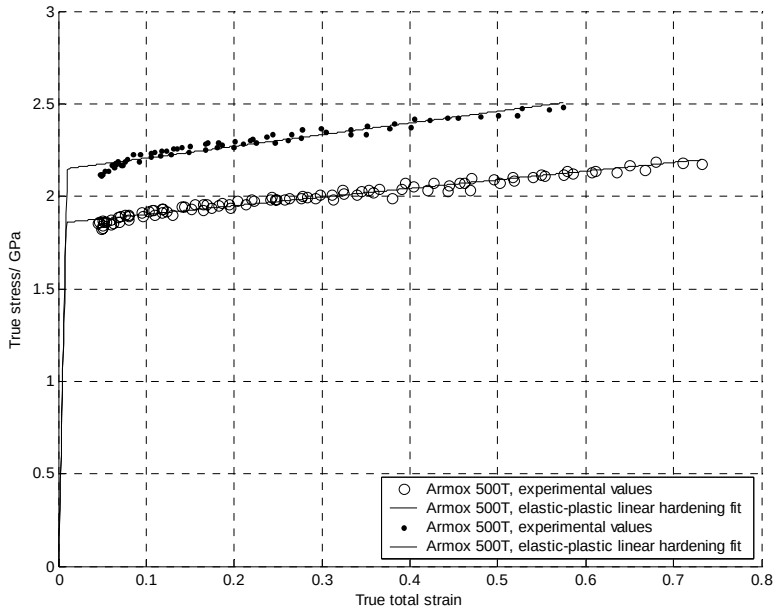

Figure 19. Data set and elastic-plastic linear hardening.

As seen in Figure 19, the elastic-plastic linear hardening model gave good agreement with the experimental data.

5.4.3 Parabolic type strain hardening

Many strength models, including all variants of Johnson & Cook, have a similar strain hardening term,

$$\sigma_Y = \left(A + B\varepsilon^n \right). \quad \textbf{(32)}$$

There is a number of ways to fit the data to the function:

- Setting $A = R_{p0.2}$ and thereby reducing the strain hardening equation to $\sigma_Y - A = B\varepsilon^n$ where the left side is know and the equation easily solvable by the least square method with one of three data sets, Figure 20 and Figure 21:
    - Using all data, i.e. both from the MTS system and the Bridgman correction.
    - Using only the data from the Bridgman correction.

- Using only the data from the MTS system.

- Not constraining A and making a fit to the data using an optimisation software with one of three data sets, Figure 22 and Figure 23:
  - Using all data, i.e. both from the MTS system and the Bridgman correction.
  - Using only the data from the Bridgman correction.
  - Using only the data from the MTS system.

These paths are explored in the following sections, 5.4.4 and 5.4.5.

5.4.4 Initial yield strength fixed

The A parameter is set equal to the $R_{P0.2}$ value from the experiments, Table 7. When A is known (32) turns into

$$\begin{aligned} &\sigma_Y = \left(A + B\varepsilon^n \right) \Rightarrow \{A \text{ known}\} \Rightarrow \\ &\sigma_Y - A = B\varepsilon^n \Rightarrow \ln\left(\sigma_Y - A\right) = \ln B + n \ln \varepsilon \end{aligned} \qquad \textbf{(33)}$$

This problem can be solved using least square method.

The results of equation (33) are shown in Figure 20 and Figure 21 and in Table 11. As can be seen, the fits of the MTS data set or fits using both data sets do not show a good over all agreement with the experimental data at high strains. The fit using the data from the Bridgman correction, i.e. stresses and strains after necking, show a good agreement with the experimental data at high strain and acceptable agreement at low strains.

Table 11. Constants describing work hardening.

	A **/GPa**	B **/GPa**	n
Armox 500T, $A = R_{p0.2}$, all data sets	1.47	1.26	0.382
Armox 500T, $A = R_{p0.2}$, MTS data set	1.47	2.37	0.505
Armox 500T, $A = R_{p0.2}$, Bridgman data set	1.47	0.702	0.199
Armox 600T, $A = R_{p0.2}$, all data sets	1.58	2.34	0.449
Armox 600T, $A = R_{p0.2}$, MTS data set	1.58	3.95	0.552
Armox 600T, $A = R_{p0.2}$, Bridgman data set	1.58	0.958	0.175

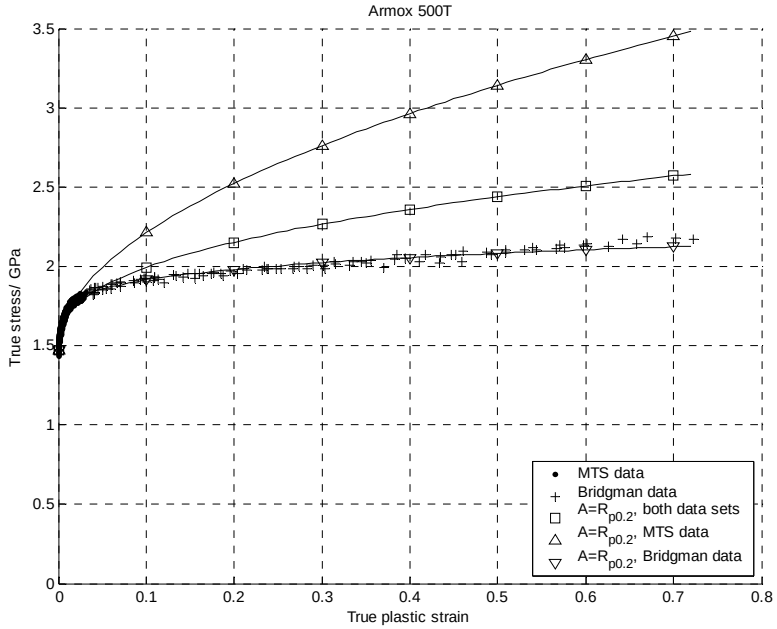

Figure 20. Armox 500T: Results from curve fitting with various data sets.

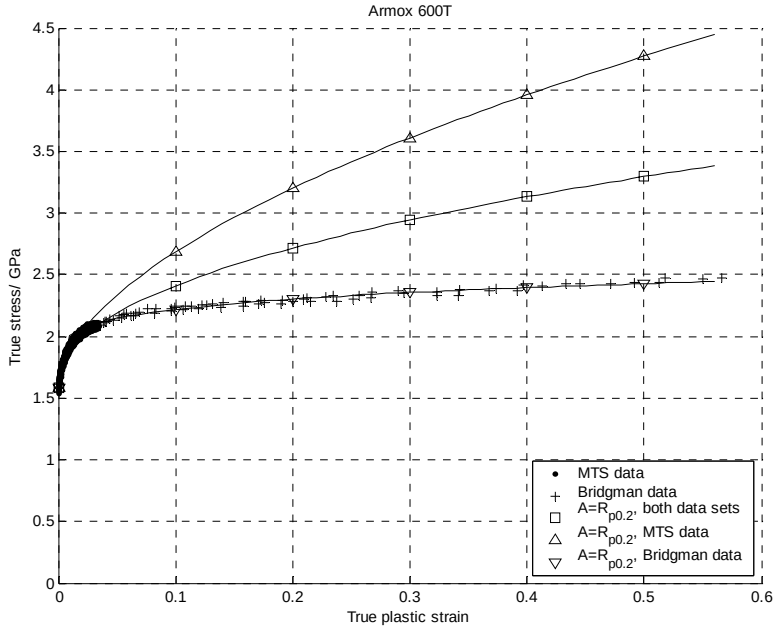

Figure 21. Armox 600T: Results from curve fitting with various data sets.

5.4.5 Initial yield strength not fixed

The fitting process utilising an optimisation software resulted in the constants shown in Table

12 and plotted in Figure 22 and Figure 23. As can be seen, the fits of the experimental data from the MTS data set do not show a good agreement with the experimental data at high strains. The fit using the data from the Bridgman correction, i.e. stresses and strains after necking, or both data sets show a good agreement with the experimental data at high strains but less god at low strains, overestimating and underestimating the yield stress, respectively.

Table 12. Constants describing strain hardening.

	A/**GPa**	B/**GPa**	n
Armox 500T, $A \neq R_{p0.2}$, both data sets	0.936	1.24	0.100
Armox 500T, $A \neq R_{p0.2}$, MTS data set	1.34	1.23	0.256
Armox 500T, $A \neq R_{p0.2}$, Bridgman data set	1.80	0.453	0.652
Armox 600T, $A \neq R_{p0.2}$, both data sets	0.828	1.79	0.105
Armox 600T, $A \neq R_{p0.2}$, MTS data set	1.41	1.87	0.285
Armox 600T, $A \neq R_{p0.2}$, Bridgman data set	1.88	0.695	0.312

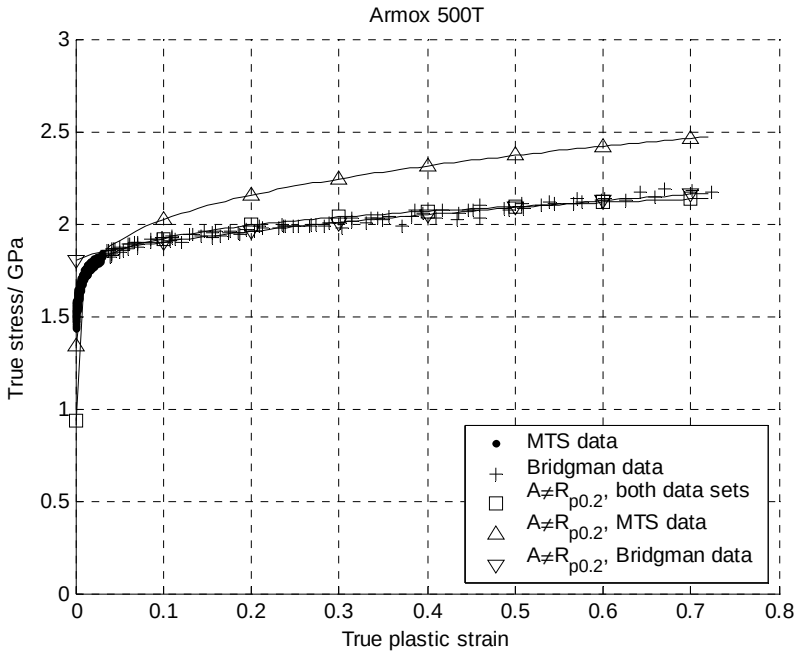

Figure 22. Armox 500T: Results from curve fitting with various data sets.

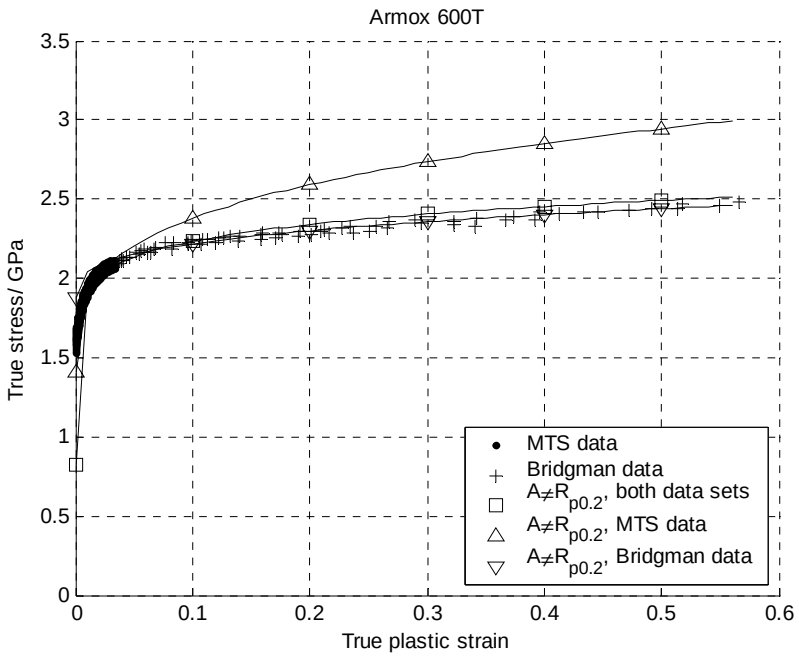

Figure 23. Armox 600T: Results from curve fitting with various data sets.

5.5 Strain rate hardening and thermal softening

The yield point at higher strain rates is misleading, since the plastic wave needs to reverberate through the sample several times before force equilibrium occurs. Because of this all data at plastic strains below 1.5% were discarded for test at strain rates higher than 1 /s, see section 3.3.2. This means that the strain rate hardening cannot be calculated from yield points, i.e. dynamic $R_{p0.2}$ values, as a function of strain rate. Trying to "go back in time" by reducing the stress at, for example, a plastic strain of 1.5% by dividing it with the strain hardening component will also be incorrect because strain rate hardening and thermal softening are coupled since tensile test at higher strain rates take place under adiabatic conditions. The best option is to use an optimisation software and fit strain rate hardening and thermal softening at the same time.

As an alternative, optimisation procedures were tested where all parameters were extracted with the optimisation software.

As a measure of the goodness of the fit, residual sum of squares,

$$RSS = \sum\left(\sigma_{\text{exp}} - \sigma_{\text{fit}}\right)^2, \tag{34}$$

and coefficient of correlation,

$$R = 1 - \frac{RSS}{\sum\left(\sigma_{\text{exp}} - \text{mean}\left(\sigma_{\text{fit}}\right)\right)^2}, \tag{35}$$

were used.

5.5.1 Armox 500T

5.5.1.1 Johnson & Cook, JC

$$\sigma_Y = \left(A + B\varepsilon^n \right)\left(1 + C \ln \frac{\dot{\varepsilon}}{\dot{\varepsilon}_0} \right)\left(1 - \left(\frac{T - T_0}{T_{melt} - T_0} \right)^m \right) \qquad \textbf{(36)}$$

Two optimisation procedures were performed:

1. $A = 1.47$ GPa, $B = 0.702$ GPa and $n = 0.199$ from 5.4.4. Data set used: all tensile tests at engineering strain rates 1 /s and higher performed at various temperatures.
2. All parameters included in the fitting process. Data set used: all tensile tests, including quasi-static and data from the Bridgman correction.

Table 13. Parameters in JC constitutive model, Armox 500T.

Parameters	Values, procedure 1	Values, procedure 2
A / GPa =	1.47 (constant)	0.849
B / GPa =	0.702 (constant)	1.34
n =	0.199 (constant)	0.0923
C =	0.00549	0.00541
m =	0.811	0.870
$RSS / 10^{18}$ =	6.88	5.12
R =	0.893	0.920

RSS and R are calculated on the results from all experiments.

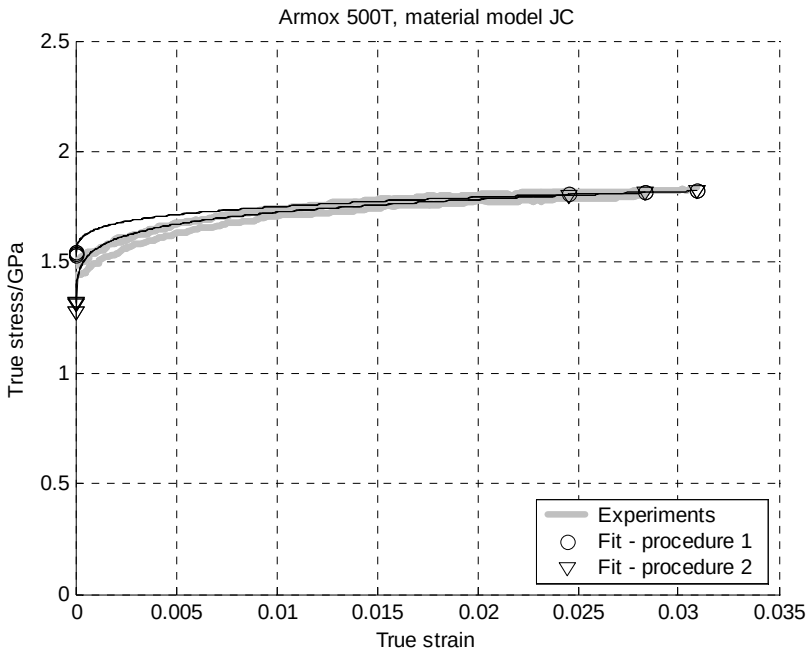

Figure 24. Fit – low strains and quasi-static. Note that the smallest strain >0.

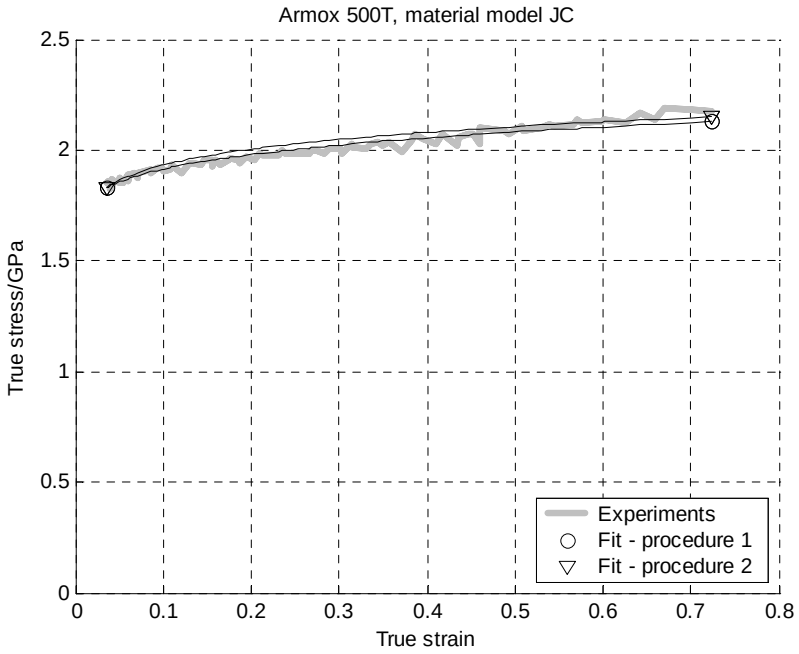

Figure 25. Fit – high strains and quasi-static.

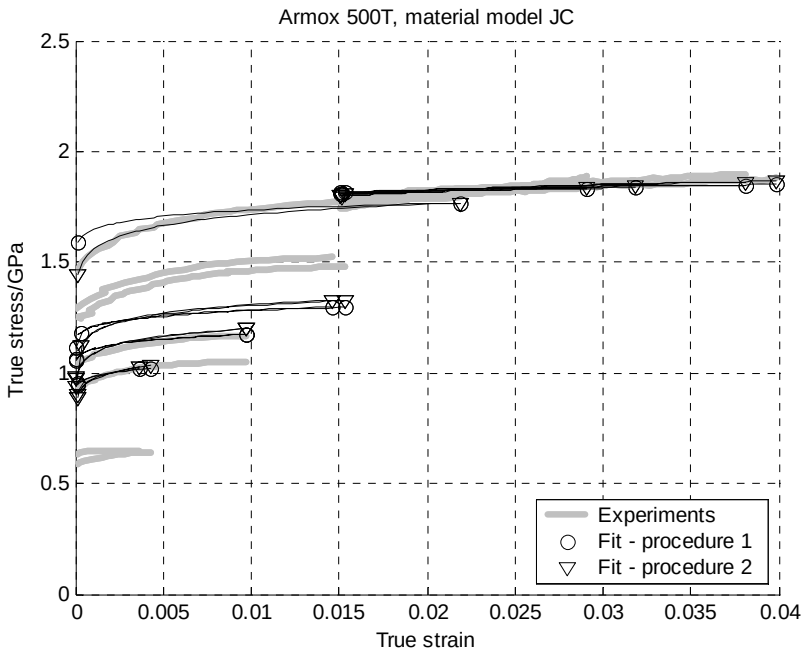

Figure 26. Fit – varying strain rates and temperatures. Note that the smallest strain >0.

5.5.1.2 Weerasooriya, JCW

$$\sigma_Y = \left(A + B\varepsilon^n \right)\left(1 + C\ln\frac{\dot{\varepsilon}}{\dot{\varepsilon}_0} \right)\left(1 - \left(\frac{T - T_0}{T_{melt} - T_0} \right) \right)^m \qquad \textbf{(37)}$$

Two optimisation procedures were performed:

1. $A = 1.47$ GPa, $B = 0.702$ GPa and $n = 0.199$ from 5.4.4. Data set used: all tensile tests at engineering strain rates 1 /s and higher performed at various temperatures.
2. All parameters included in the fitting process. Data set used: all tensile tests, including quasi-static and data from the Bridgman correction.

Table 14. Parameters in JCW constitutive model, Armox 500T.

Parameters	Values, procedure 1	Values, procedure 2
A / GPa =	1.47 (constant)	0.899
B / GPa =	0.702 (constant)	1.28
n =	0.199 (constant)	0.0958
C =	0.00411	0.00457
m =	1.44	1.32
$RSS/10^{18}$ =	6.17	4.65
R =	0.904	0.927

RSS and R are calculated on the results from all experiments.

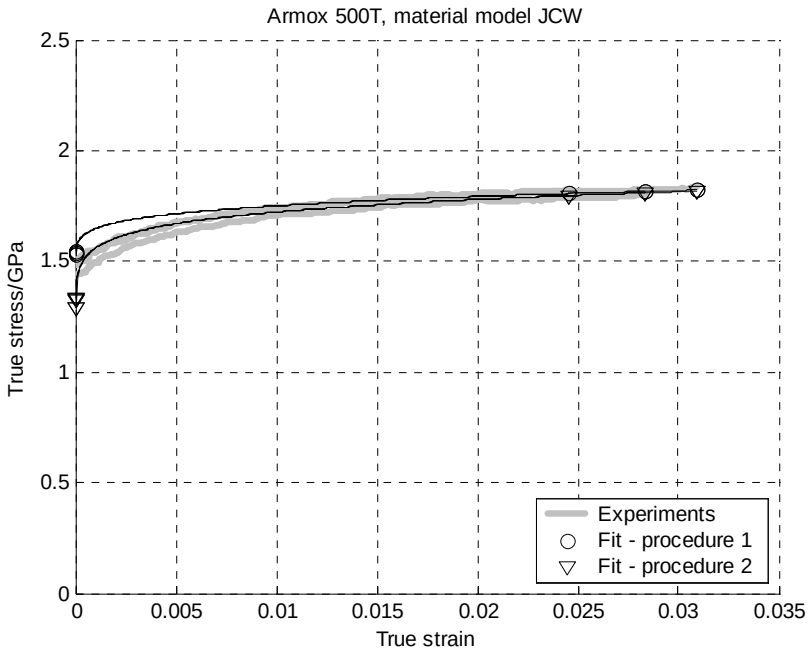

Figure 27. Fit – low strains and quasi-static. Note that the smallest strain >0.

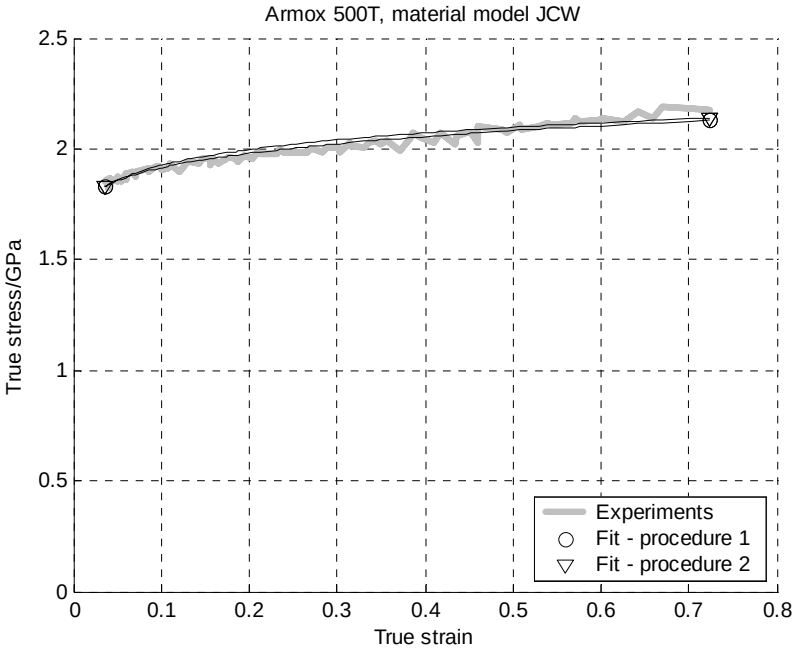

Figure 28. Fit – high strains and quasi-static.

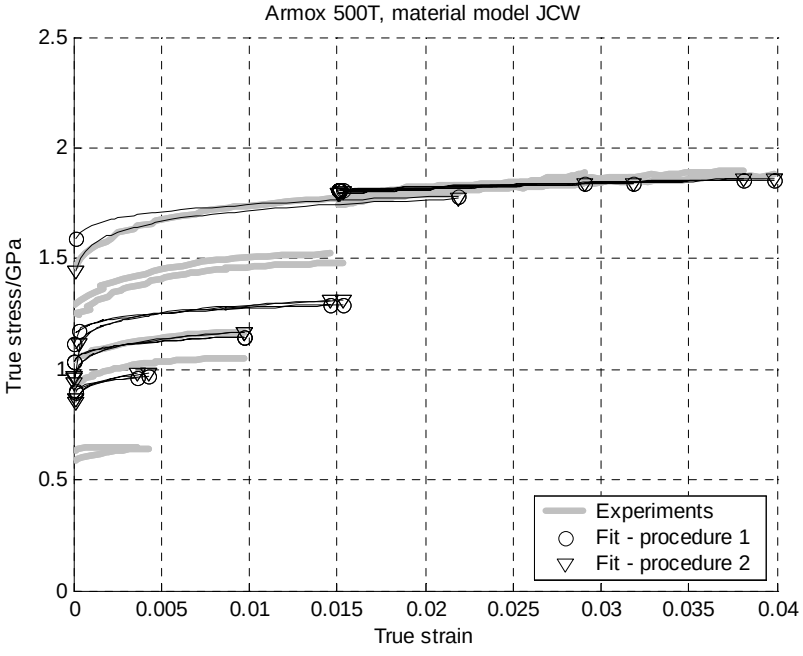

Figure 29. Fit – varying strain rates and temperatures. Note that the smallest strain >0.

5.5.1.3 Huang & Liang, HL

$$\sigma_Y = \left(A + B\varepsilon^n \right)\left(1 + C \ln \frac{\dot{\varepsilon}}{\dot{\varepsilon}_0} \right)\left(D - E\left(\frac{T - T_0}{T_{melt} - T_0} \right)^m \right) \quad \textbf{(38)}$$

Four optimisation procedures were performed:

1. $A = 1.47$ GPa, $B = 0.702$ GPa and $n = 0.199$ from 5.4.4. Data set used: all tensile tests at engineering strain rates 1 /s and higher performed at various temperatures.
2. All parameters included in the fitting process. Data set used: all tensile tests, including quasi-static and data from the Bridgman correction.
3. $A = 1.47$ GPa, $B = 0.702$ GPa and $n = 0.199$ from 5.4.4 and $D = 1$. Data set used: all tensile tests at engineering strain rates 1 /s and higher performed at various temperatures.
4. Constant D, $D = 1$. All other parameters included in the fitting process. Data set used: all tensile tests, including quasi-static and data from the Bridgman correction.

Table 15. Parameters in HL constitutive model, Armox 500T.

Parameters	Values, procedure 1	Values, procedure 2	Values, procedure 3	Values, procedure 4
A / GPa =	1.47 (constant)	0.992	1.47 (constant)	1.01
B / GPa =	0.702 (constant)	1.16	0.702 (constant)	1.18
n =	0.199 (constant)	0.110	0.199 (constant)	0.110
C =	0.00465	0.00343	0.00231	0.00343
D =	0.986	1.02	1 (constant)	1 (constant)
E =	10.2	11.7	9.42	11.5
m =	2.49	2.60	2.40	2.60
$RSS / 10^{18}$ =	1.98	1.00	2.56	1.00
R =	0.969	0.984	0.960	0.984

RSS and R are calculated on the results from all experiments.

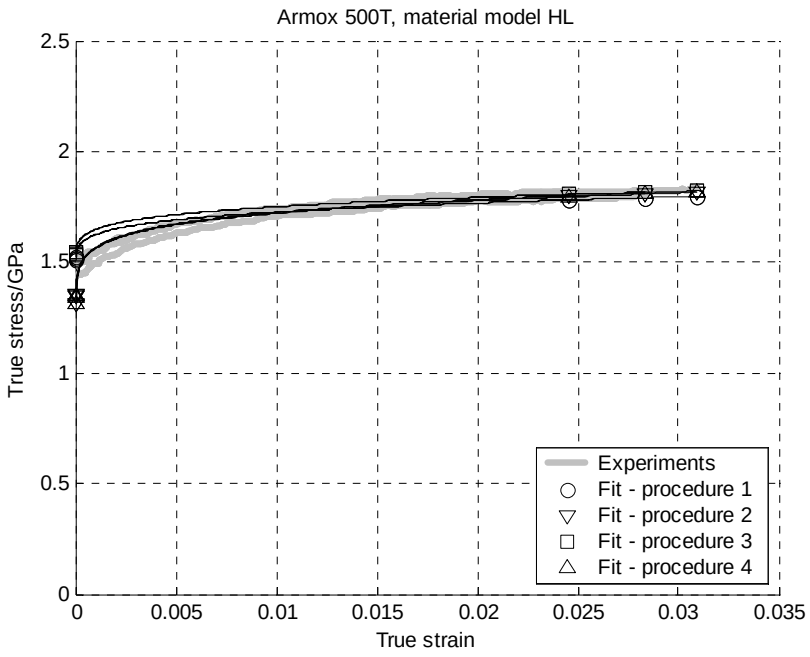

Figure 30. Fit – low strains and quasi-static. Note that the smallest strain >0.

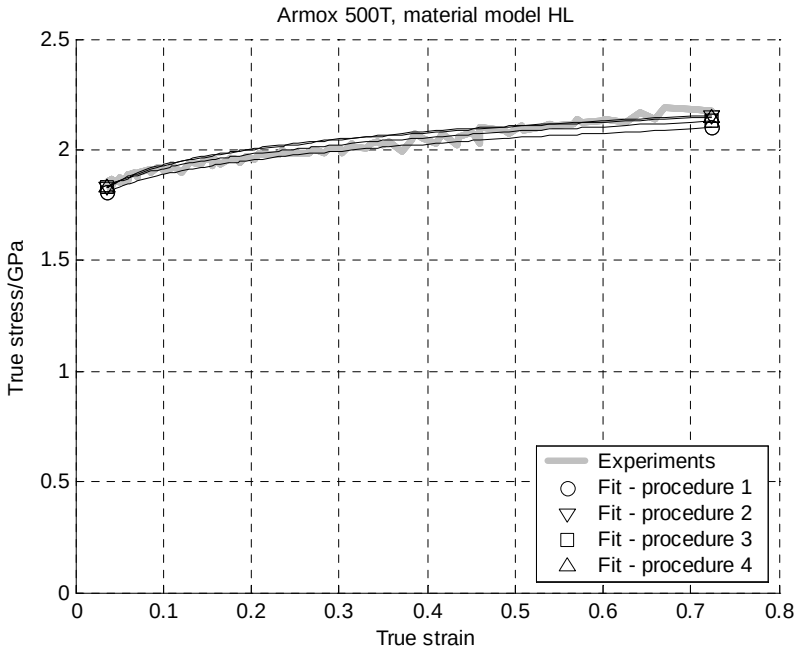

Figure 31. Fit – high strains and quasi-static.

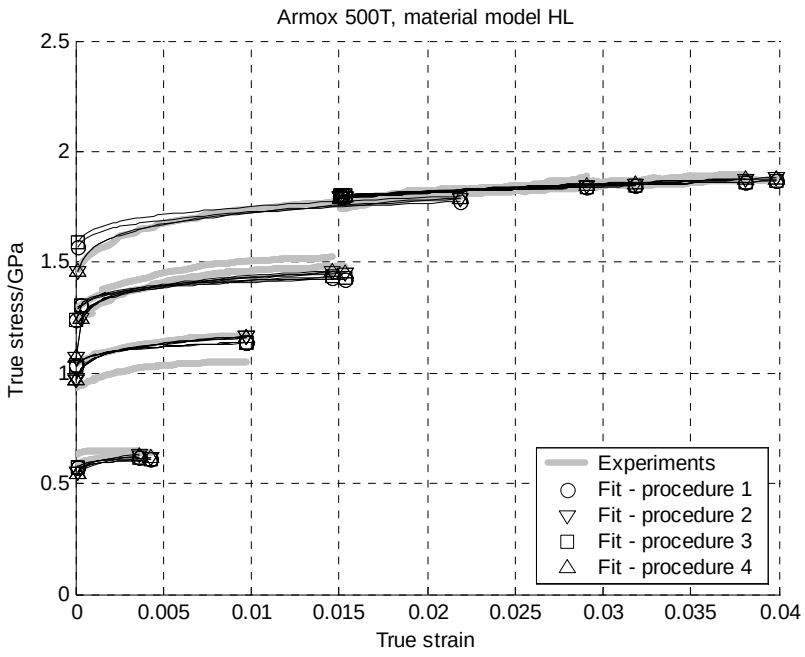

Figure 32. Fit – varying strain rates and temperatures. Note that the smallest strain >0.

5.5.1.4 Zerilli & Armstrong, ZA

$$\sigma_Y = \sigma_G + C_1 \exp\left(-C_3 T + C_4 T \ln\frac{\dot{\varepsilon}}{\dot{\varepsilon}_0}\right) + C_5 \varepsilon^n \qquad \textbf{(39)}$$

Three optimisation procedures were performed:

1. $\sigma_G = 1.47$ GPa, $C_5 = 0.702$ GPa and $n = 0.199$ from 5.4.4. Data set used: all tensile tests at engineering strain rates 1 /s and higher performed at various temperatures.
2. Including σ_G in the fitting process will result in $\sigma_G \to -\infty$ while $C_1 \to \infty$ and therefore σ_G was set constant, $\sigma_G = 0$. $C_5 = 0.702$ GPa and $n = 0.199$ from 5.4.4. Data set used: all tensile tests, including quasi-static and data from the Bridgman correction.
3. All parameters included in the fitting process except σ_G. σ_G was set constant, $\sigma_G = 0$. Data set used: all tensile tests, including quasi-static and data from the Bridgman correction.

Table 16. Parameters in ZA constitutive model, Armox 500T.

Parameters	Values, procedure 1	Values, procedure 2	Values, procedure 3
σ_G / GPa =	1.47 (constant)	0 (constant)	0 (constant)
C_5 / GPa =	0.702 (constant)	0.702 (constant)	0.973
n =	0.199 (constant)	0.199 (constant)	0.159
C_1 / GPa =	0.00203	2.23	1.97
C_3 / K =	0.00668	0.00135	0.00145
C_4 / K =	0.00246	0.00000676	0.0000136
RSS /10^{18} =	45.4	7.00	5.16
R =	0.363	0.892	0.920

RSS and R are calculated on the results from all experiments.

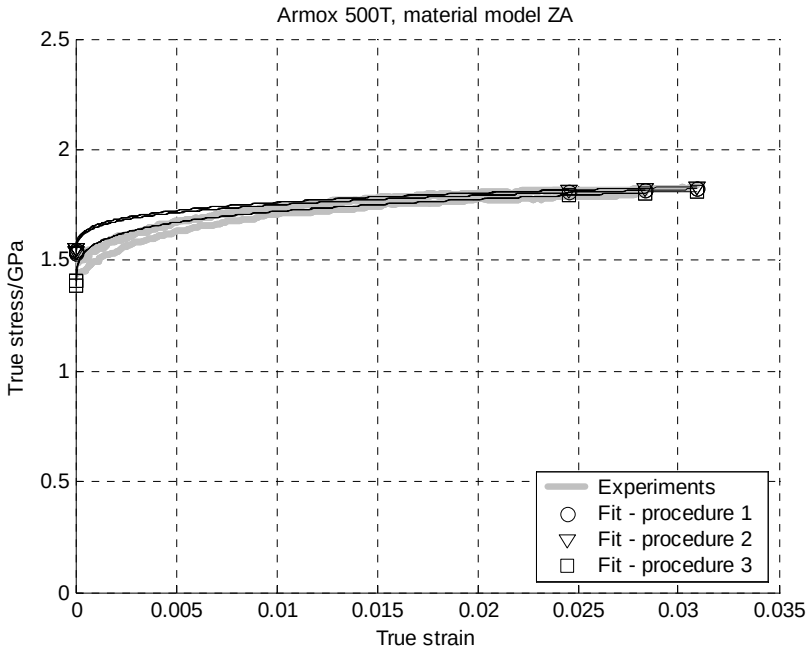

Figure 33. Fit – low strains and quasi-static. Note that the smallest strain >0.

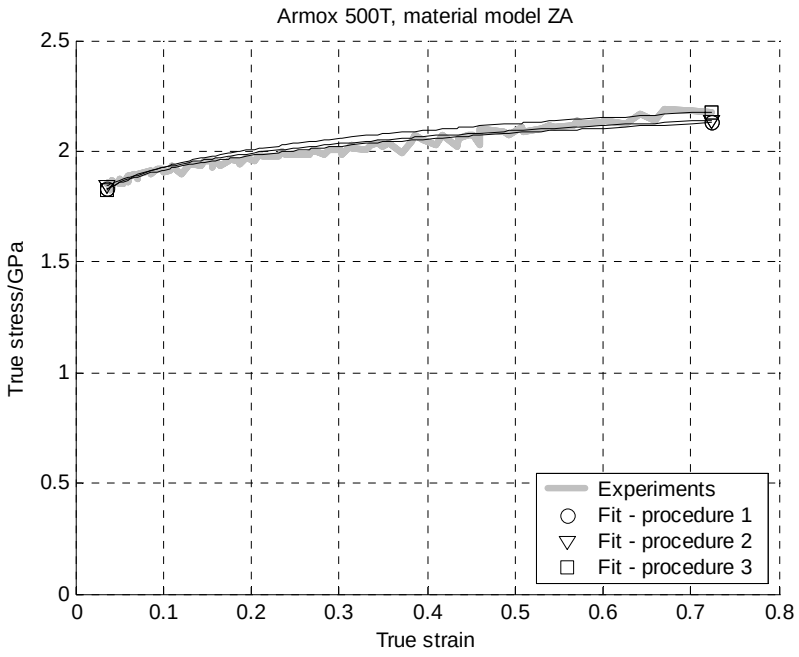

Figure 34. Fit – high strains and quasi-static.

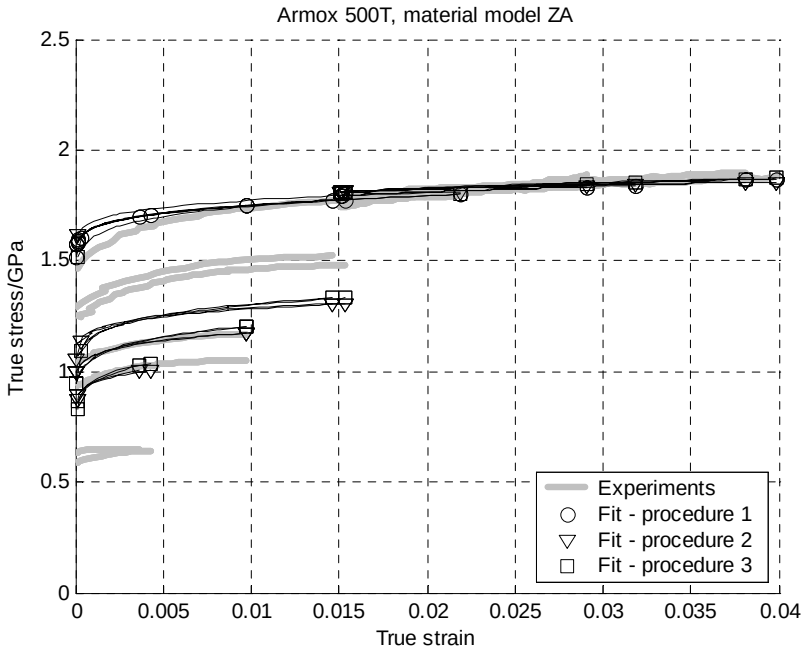

Figure 35. Fit – varying strain rates and temperatures. Note that the smallest strain >0.

From the plot above it is clear that the results from the optimisation in procedure 1 are useless, the function does not capture the thermal softening of the material at all.

5.5.2 Armox 600T

5.5.2.1 Johnson & Cook, JC

$$\sigma_Y = \left(A + B\varepsilon^n\right)\left(1 + C\ln\frac{\dot{\varepsilon}}{\dot{\varepsilon}_0}\right)\left(1 - \left(\frac{T - T_0}{T_{melt} - T_0}\right)^m\right) \qquad \textbf{(40)}$$

Two optimisation procedures were performed:

1. $A = 1.58$ GPa, $B = 0.958$ GPa and $n = 0.175$ from 5.4.4. Data set used: all tensile tests at engineering strain rates 1 /s and higher performed at various temperatures.
2. All parameters included in the fitting process. Data set used: all tensile tests, including quasi-static and data from the Bridgman correction.

Table 17. Parameters in JC constitutive model, Armox 600T.

Parameters	Values, procedure 1	Values, procedure 2
A / GPa =	1.58 (constant)	0.944
B / GPa =	0.958 (constant)	1.70
n =	0.175 (constant)	0.119
C =	0.00877	0.00962
m =	0.712	0.805
$RSS / 10^{18}$ =	11.2	4.58
R =	0.893	0.955

RSS and R are calculated on the results from all experiments.

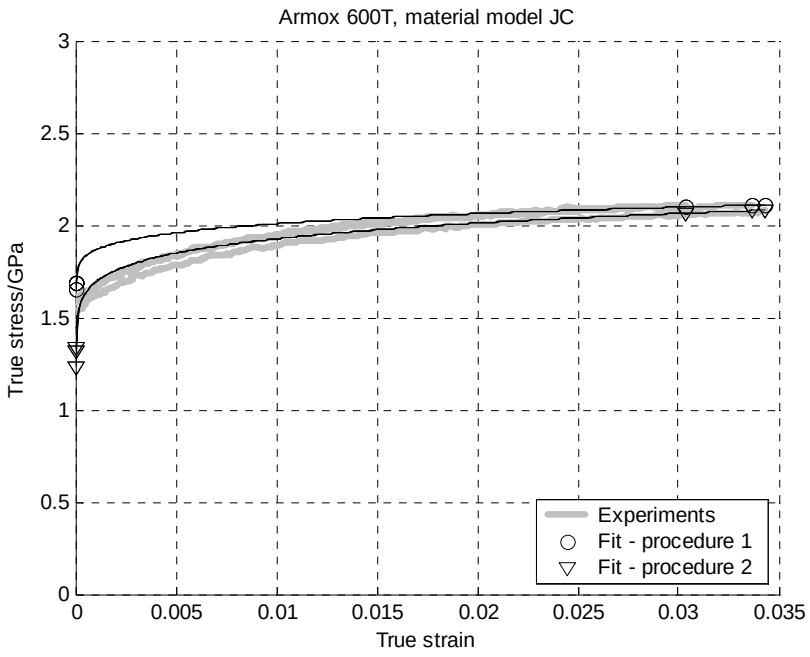

Figure 36. Fit – low strains and quasi-static. Note that the smallest strain >0.

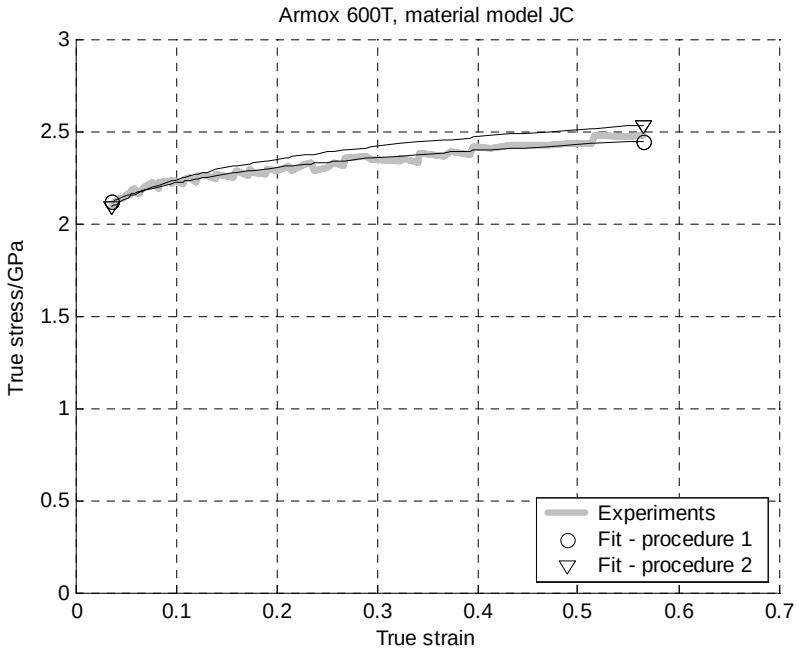

Figure 37. Fit – high strains and quasi-static.

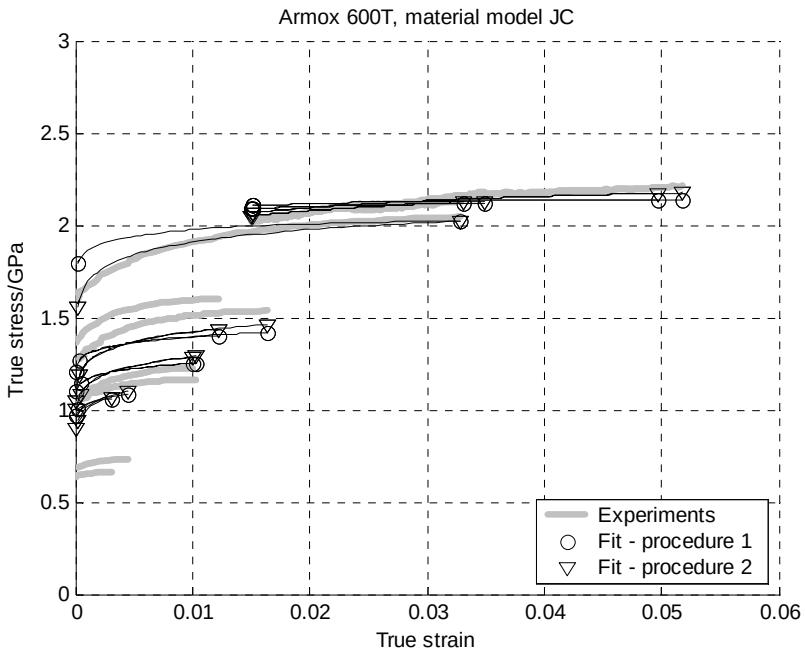

Figure 38. Fit – varying strain rates and temperatures. Note that the smallest strain >0.

5.5.2.2 Weerasooriya, JCW

$$\sigma_Y = \left(A + B\varepsilon^n \right)\left(1 + C\ln\frac{\dot{\varepsilon}}{\dot{\varepsilon}_0} \right)\left(1 - \left(\frac{T - T_0}{T_{melt} - T_0} \right) \right)^m \qquad \textbf{(41)}$$

Two optimisation procedures were performed:

1. $A = 1.58$ GPa, $B = 0.958$ GPa and $n = 0.175$ from 5.4.4. Data set used: all tensile tests at engineering strain rates 1 /s and higher performed at various temperatures.
2. All parameters included in the fitting process. Data set used: all tensile tests, including quasi-static and data from the Bridgman correction.

Table 18. Parameters in JCW constitutive model, Armox 600T.

Parameters	Values, procedure 1	Values, procedure 2
A / GPa =	1.58 (constant)	0.976
B / GPa =	0.958 (constant)	1.66
n =	0.175 (constant)	0.121
C =	0.00511	0.00785
m =	1.72	1.47
$RSS/10^{18}$ =	10.1	3.90
R =	0.903	0.962

RSS and R are calculated on the results from all experiments.

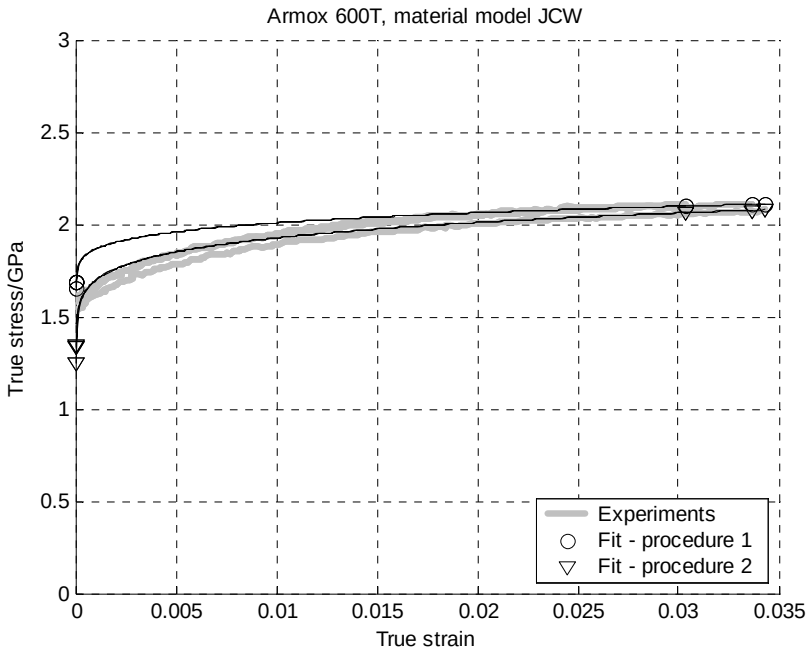

Figure 39. Fit – low strains and quasi-static. Note that the smallest strain >0.

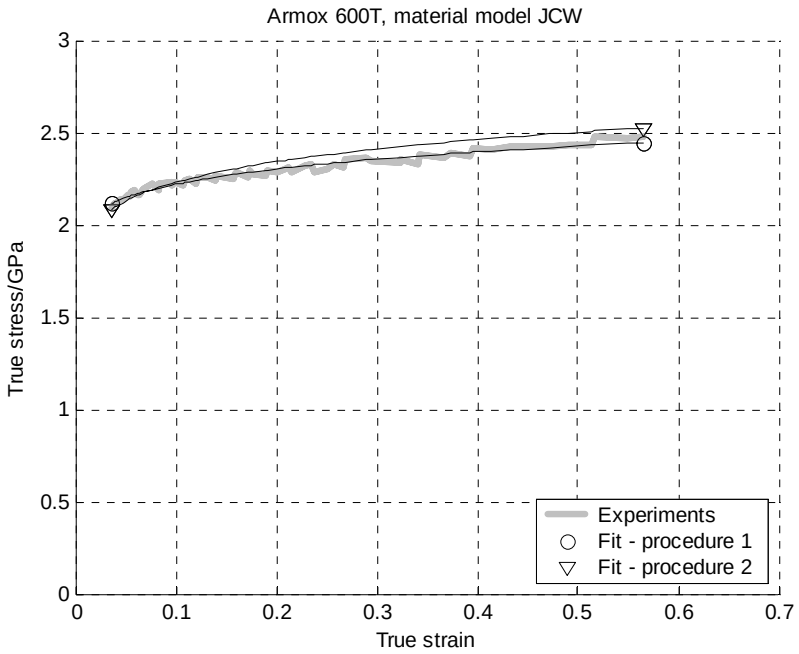

Figure 40. Fit – high strains and quasi-static.

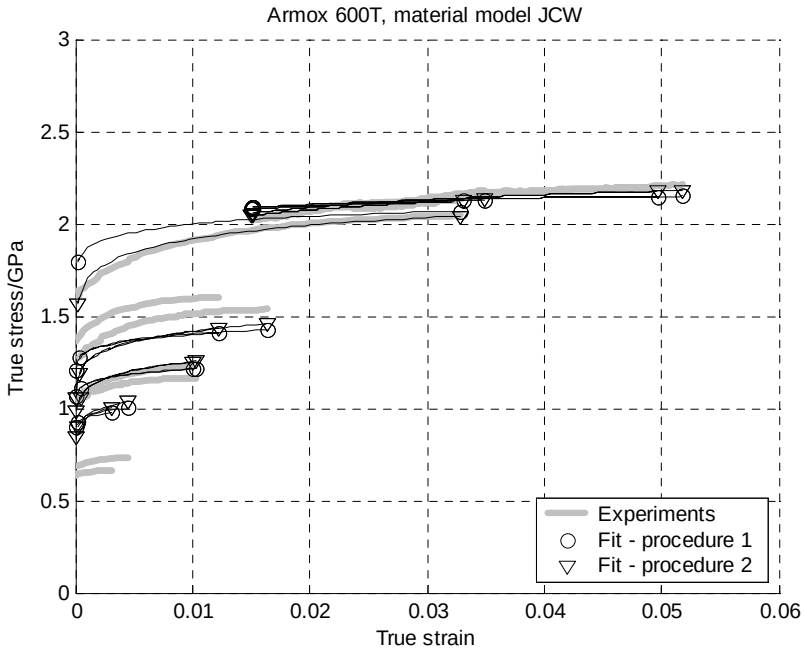

Figure 41. Fit – varying strain rates and temperatures. Note that the smallest strain >0.

5.5.2.3 Huang & Liang, HL

$$\sigma_Y = \left(A + B\varepsilon^n \right)\left(1 + C \ln \frac{\dot{\varepsilon}}{\dot{\varepsilon}_0} \right)\left(D - E\left(\frac{T - T_0}{T_{melt} - T_0} \right)^m \right) \quad \textbf{(42)}$$

Four optimisation procedures were performed:

1. $A = 1.58$ GPa, $B = 0.958$ GPa and $n = 0.175$ from 5.4.4. Data set used: all tensile tests at engineering strain rates 1 /s and higher performed at various temperatures.
2. All parameters included in the fitting process. Data set used: all tensile tests, including quasi-static and data from the Bridgman correction.
3. $A = 1.58$ GPa, $B = 0.958$ GPa and $n = 0.175$ from 5.4.4, $D = 1$. Data set used: all tensile tests at engineering strain rates 1 /s and higher performed at various temperatures.
4. Constant D, $D = 1$. All other parameters included in the fitting process. Data set used: all tensile tests, including quasi-static and data from the Bridgman correction.

Table 19. Parameters in HL constitutive model, Armox 600T.

Parameters	Values, procedure 1	Values, procedure 2	Values, procedure 3	Values, procedure 4
A / GPa =	1.58 (constant)	0.943	1.58 (constant)	1.02
B / GPa =	0.958 (constant)	1.49	0.958 (constant)	1.62
n =	0.175 (constant)	0.126	0.175 (constant)	0.126
C =	0.0118	0.00577	0.00239	0.00577
D =	0.948	1.09	1 (constant)	1 (constant)
E =	5.78	6.58	4.59	6.06
m =	2.03	2.04	1.76	2.04
$RSS / 10^{18}$ =	5.34	1.56	8.02	1.56
R =	0.948	0.985	0.923	0.985

RSS and R are calculated on the results from all experiments.

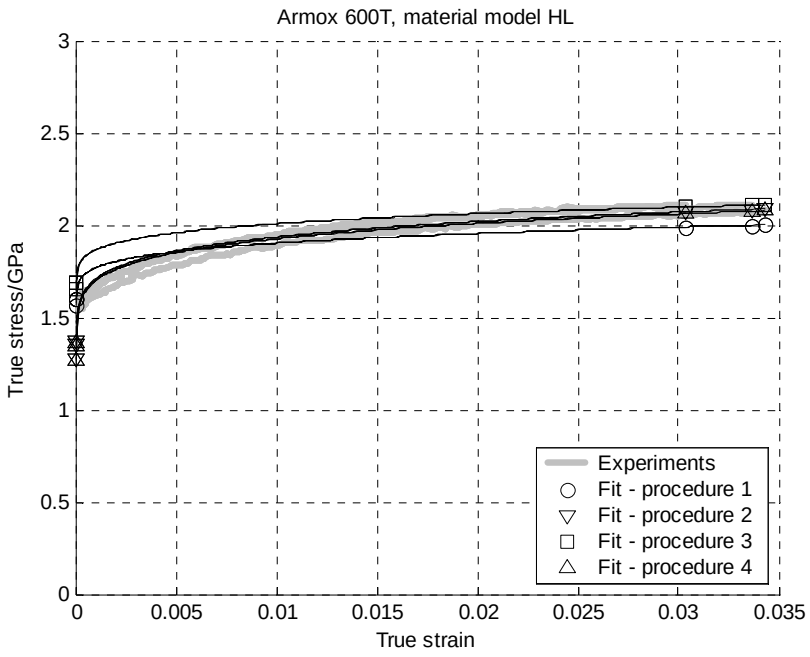

Figure 42. Fit – low strains and quasi-static. Note that the smallest strain >0.

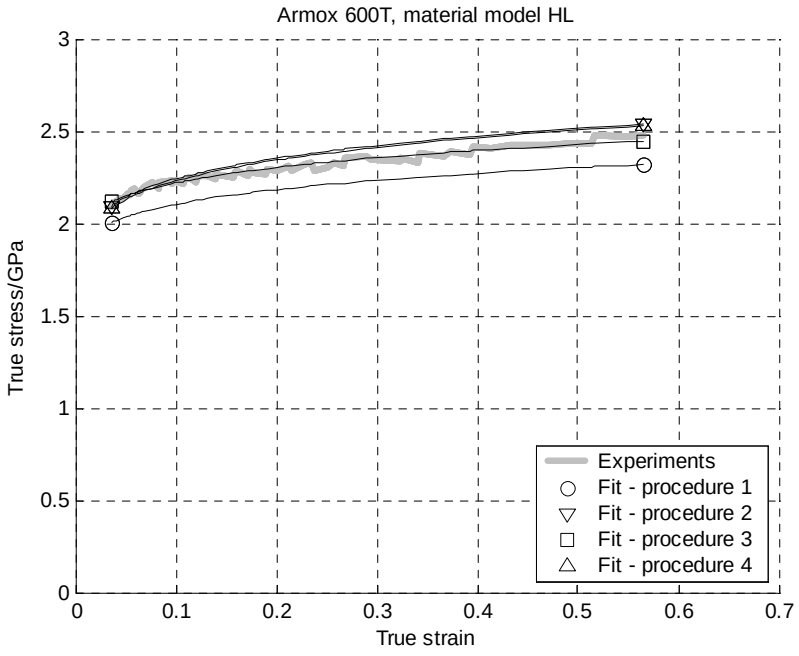

Figure 43. Fit – high strains and quasi-static.

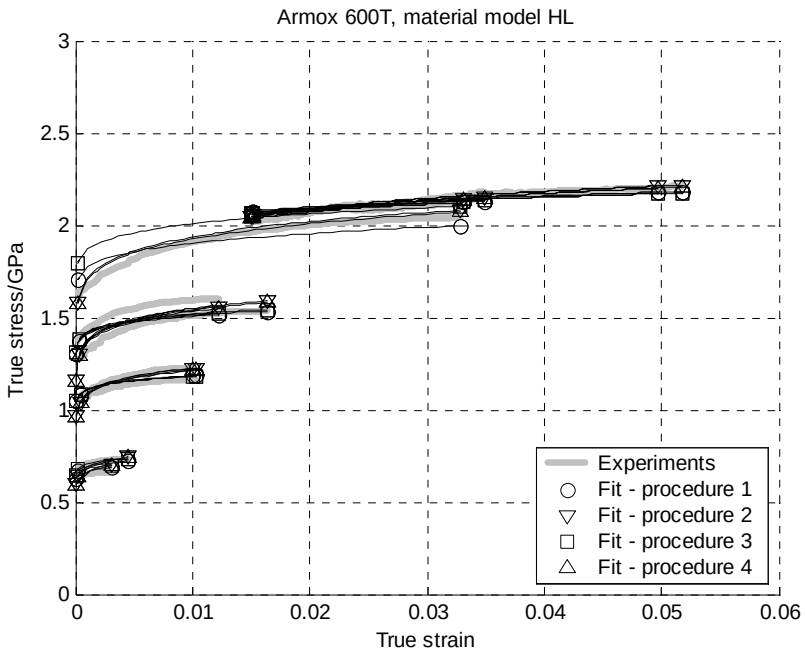

Figure 44. Fit – varying strain rates and temperatures. Note that the smallest strain >0.

5.5.2.4 Zerilli & Armstrong, ZA

$$\sigma_Y = \sigma_G + C_1 \exp\left(-C_3 T + C_4 T \ln\frac{\dot{\varepsilon}}{\dot{\varepsilon}_0}\right) + C_5 \varepsilon^n \qquad \textbf{(43)}$$

Three optimisation procedures were performed:

1. $\sigma_G = 1.58$ GPa, $C_5 = 0.958$ GPa and $n = 0.175$ from 5.4.4. Data set used: all tensile tests at engineering strain rates 1 /s and higher performed at various temperatures.
2. Including σ_G in the fitting process will result in $\sigma_G \to -\infty$ while $C_1 \to \infty$ and therefore σ_G was set constant, $\sigma_G = 0$. $C_5 = 0.958$ GPa and $n = 0.175$ from 5.4.4. Data set used: all tensile tests, including quasi-static and data from the Bridgman correction.
3. All parameters included in the fitting process. Data set used: all tensile tests, including quasi-static and data from the Bridgman correction.

Table 20. Parameters in ZA constitutive model, Armox 600T.

Parameters	Values, procedure 1	Values, procedure 2	Values, procedure 3
σ_G / GPa =	1.58 (constant)	0 (constant)	0 (constant)
C_5 / GPa =	0.958 (constant)	0.958 (constant)	1.41
n =	0.175 (constant)	0.175 (constant)	0.174
C_1 / GPa =	-0.0000591	0.000561	2.27
C_3 / K =	2.10	-0.00696	0.00180
C_4 / K =	0.258	0.00192	0.0000206
RSS /10^{18} =	72.6	2522	4.79
R =	0.372	0.0185	0.953

RSS and R are calculated on the results from all experiments.

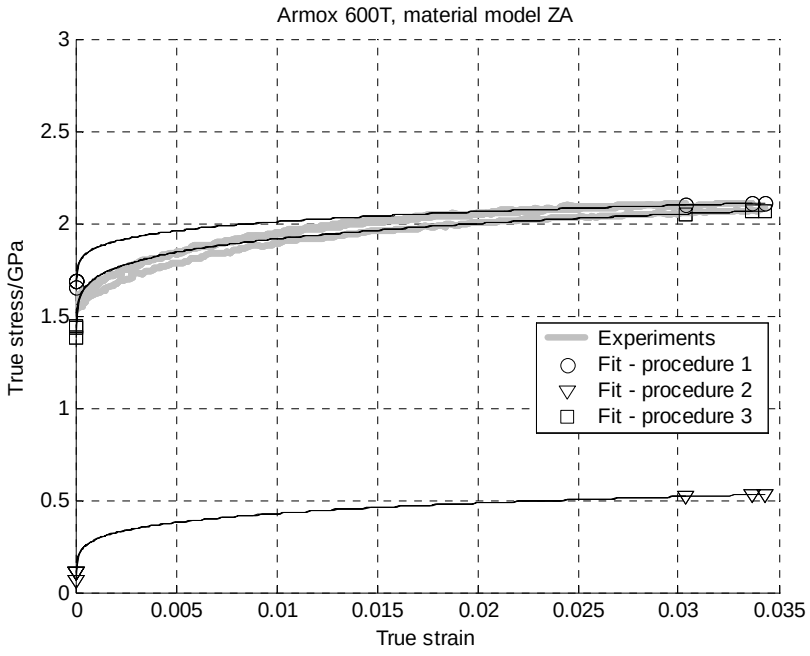

Figure 45. Fit – low strains and quasi-static. Note that the smallest strain >0.

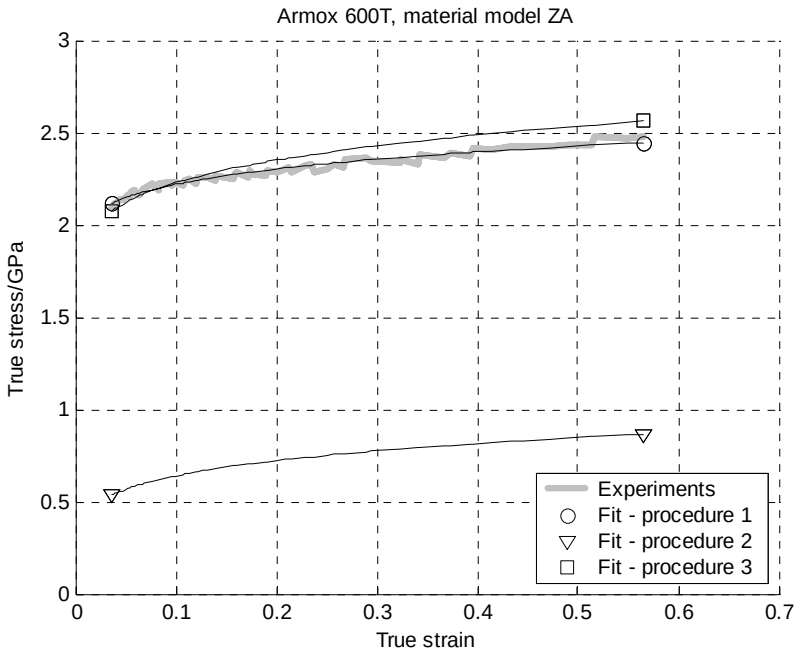

Figure 46. Fit – high strains and quasi-static.

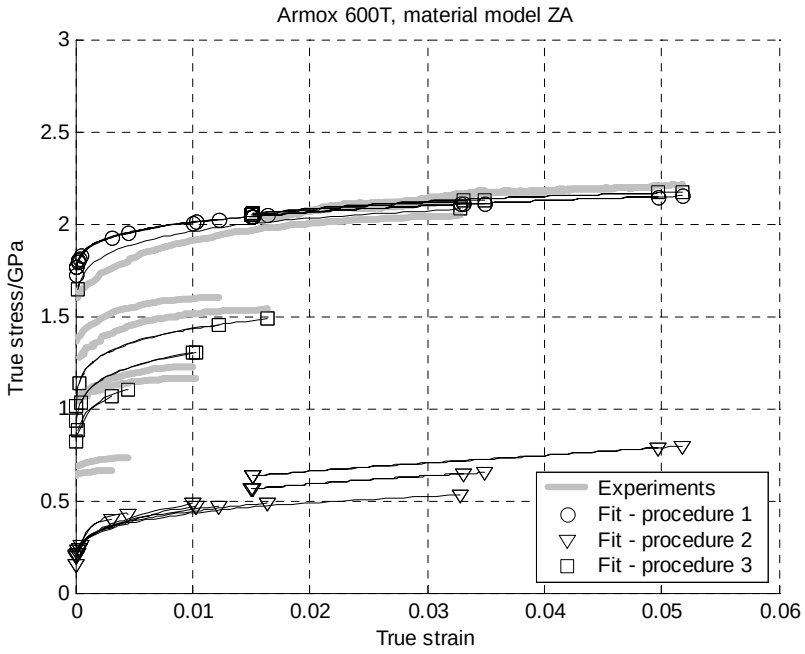

Figure 47. Fit – varying strain rates and temperatures. Note that the smallest strain >0.

From the plots above it is clear that the results from the optimisation in procedure 1 and 2 does not capture the behaviour of the material at all.

From what has been shown above, it is clear that the procedure for extracting the parameters is important. The same experimental data will produce different sets of parameters depending

on how the optimisation process was carried out. But it is equally important to make sure that the parameter set does not cause unphysical behaviour in the vicinity of the experimental room. Extrapolating to high strain at constant strain rate and checking isothermal and adiabatic conditions will reveal faults in the parameter sets.

For the case of Armox 500T, the strength model ZA and procedure 1 produced erroneous results and was discarded. In Figure 48 the results of all remaining strength models and procedures for Armox 500T are plotted for isothermal conditions, i.e. the thermal softening is turned off, and at a strain rate of 1000 /s. It seems like the differences between different strength models and procedures are small.

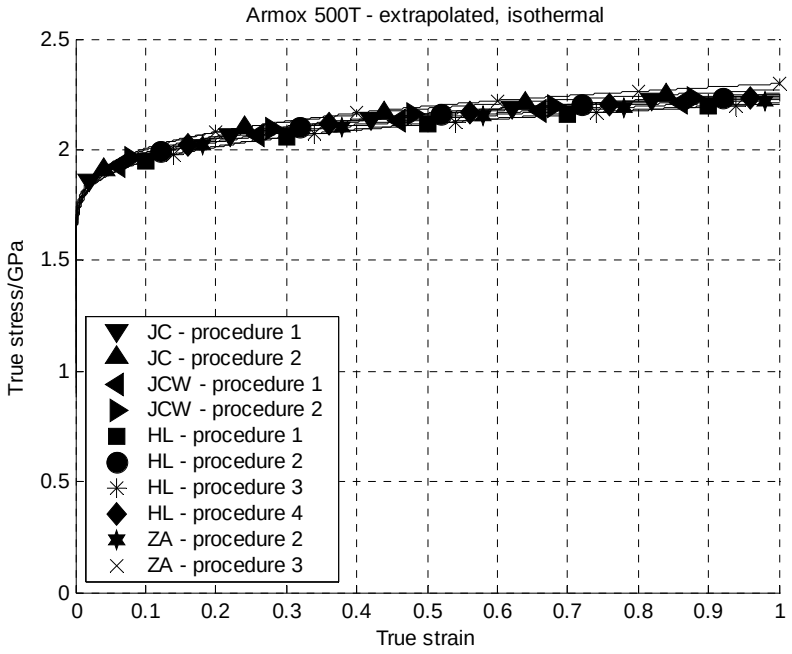

Figure 48. All models and procedures – Armox 500T. Strain rate 1000 /s, isothermal conditions.

In Figure 49 the results of all strength models and procedures for Armox 500T are plotted for adiabatic conditions, i.e. 90% of plastic work is transformed into heat, and at a strain rate of 1000 /s. The differences between different strength models and procedures are significant.

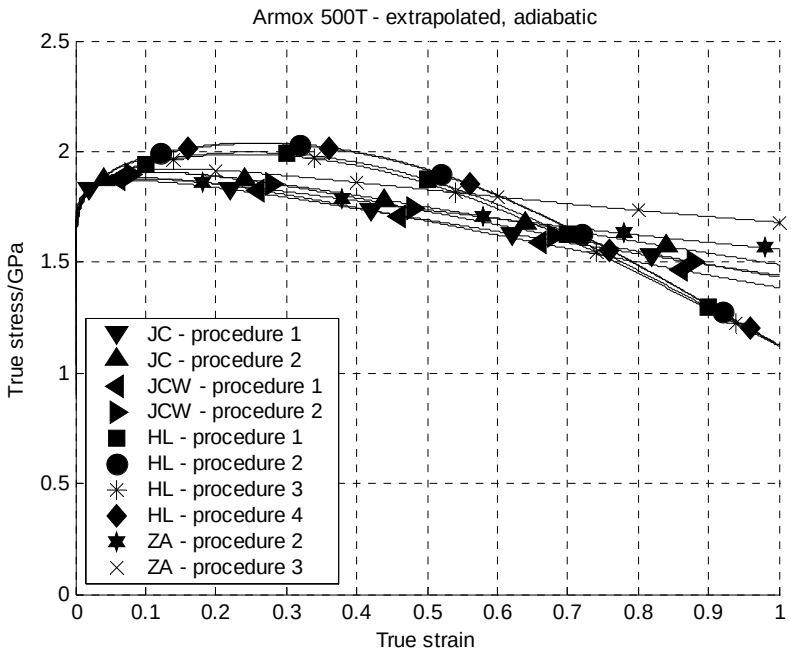

Figure 49. All models and procedures – Armox 500T. Strain rate 1000 /s, adiabatic conditions.

For the case of Armox 600T, the strength model ZA and procedure 1 and 2 produced erroneous results and were discarded. Plotting the results of the strength models and the remaining procedures at isothermal conditions, i.e. the thermal softening is turned off, and at a strain rate of 1000 /s, Figure 50, shows a larger difference between different strength models and procedures than in the Armox 500T case.

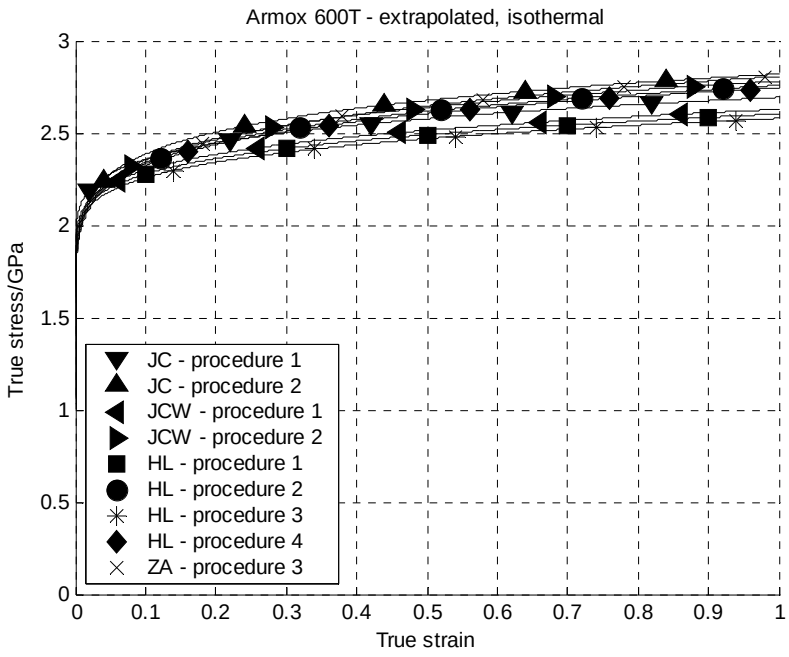

Figure 50. All models and procedures – Armox 600T. Strain rate 1000 /s, isothermal conditions.

Plotting the results of all strength models and procedures for Armox 600T at adiabatic conditions, i.e. 90% of plastic work is transformed into heat, and at a strain rate of 1000 /s, Figure 51, gives a similar result as with Armox 500T. The differences between different strength models and procedures are significant.

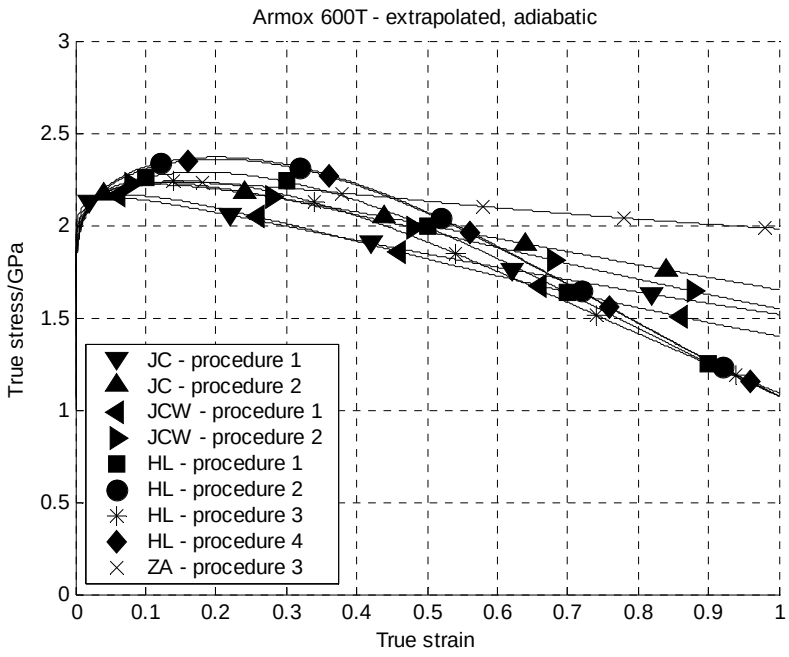

Figure 51. All models and procedures – Armox 600T. Strain rate 1000 /s, adiabatic conditions.

After this check of validity the valid strength models and procedures giving reasonable results are listed in Table 21 (JC), Table 22 (JCW), Table 23 (HL) and Table 24 (ZA).

Table 21. Johnson & Cook.

	Armox 500T		**Armox 600T**	
Parameters	Values, procedure 1	Values, procedure 2	Values, procedure 1	Values, procedure 2
A / GPa =	1.47	0.849	1.58	0.944
B / GPa =	0.702	1.34	0.958	1.70
n =	0.199	0.0923	0.175	0.119
C =	0.00549	0.00541	0.00877	0.00962
m =	0.811	0.870	0.712	0.805
$RSS/10^{18}$ =	6.88	5.12	11.2	4.58
R =	0.893	0.920	0.893	0.955

Table 22. Weerasooriya.

	Armox 500T		Armox 600T	
Parameters	Values, procedure 1	Values, procedure 2	Values, procedure 1	Values, procedure 2
A / GPa =	1.47	0.899	1.58	0.976
B / GPa =	0.702	1.28	0.958	1.66
n =	0.199	0.0958	0.175	0.121
C =	0.00411	0.00457	0.00511	0.00785
m =	1.44	1.32	1.72	1.47
$RSS/10^{18}$ =	6.17	4.65	10.1	3.90
R =	0.904	0.927	0.903	0.962

Table 23. Huang & Liang.

	Armox 500T				Armox 600T			
Parameters	Values, procedure 1	Values, procedure 2	Values, procedure 3	Values, procedure 4	Values, procedure 1	Values, procedure 2	Values, procedure 3	Values, procedure 4
A / GPa =	1.47	0.992	1.47	1.01	1.58	0.943	1.58	1.02
B / GPa =	0.702	1.16	0.702	1.18	0.958	1.49	0.958	1.62
n =	0.199	0.110	0.199	0.110	0.175	0.126	0.175	0.126
C =	0.00465	0.00343	0.00231	0.00343	0.0118	0.00577	0.00239	0.00577
D =	0.986	1.02	1	1	0.948	1.09	1	1
E =	10.2	11.7	9.42	11.5	5.78	6.58	4.59	6.06
m =	2.49	2.60	2.40	2.60	2.03	2.04	1.76	2.04
$RSS/10^{18}$ =	1.98	1.00	2.56	1.00	5.34	1.56	8.02	1.56
R =	0.969	0.984	0.960	0.984	0.948	0.985	0.923	0.985

Table 24. Zerilli & Armstrong.

	Armox 500T		**Armox 600T**
Parameters	Values, procedure 2	Values, procedure 3	Values, procedure 3
σ_G / GPa =	0	0	0
C_5 / GPa =	0.702	0.973	1.41
n =	0.199	0.159	0.174
C_1 / GPa =	2.23	1.97	2.27
C_3 / K =	0.00135	0.00145	0.00180
C_4 / K =	0.00000676	0.0000136	0.0000206
$RSS / 10^{18}$ =	7.00	5.16	4.79
R =	0.892	0.920	0.953

6 Discussion

Using the same data but different strength models and different procedures to derive the parameters in the strength models will result in different material behaviour at the vicinity of the experimental room. Under isothermal conditions the difference between the strength models are small, almost insignificant, but under adiabatic conditions, i.e. real conditions, the difference between the strength models and the different procedures to extract the material parameters are significant, Figure 49 and Figure 51.

In Figure 52 and Figure 53 the yield strengths, at a strain of 0.1%, a strain rate of 1 /s and temperatures between room temperature and melting temperature, of the various models and procedures are plotted together with the experimental data.

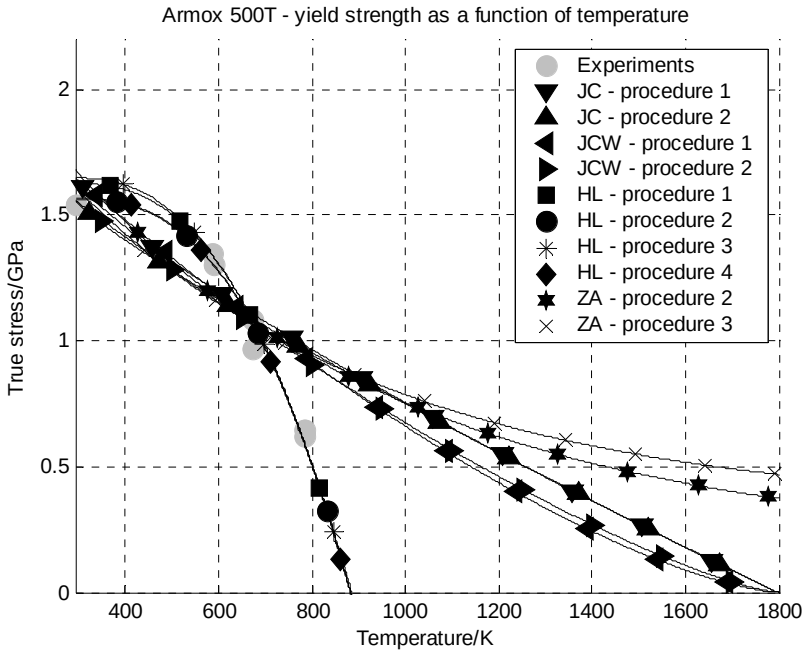

Figure 52. Yield strength at 0.1% strain, a strain rate of 1 /s and various temperatures.

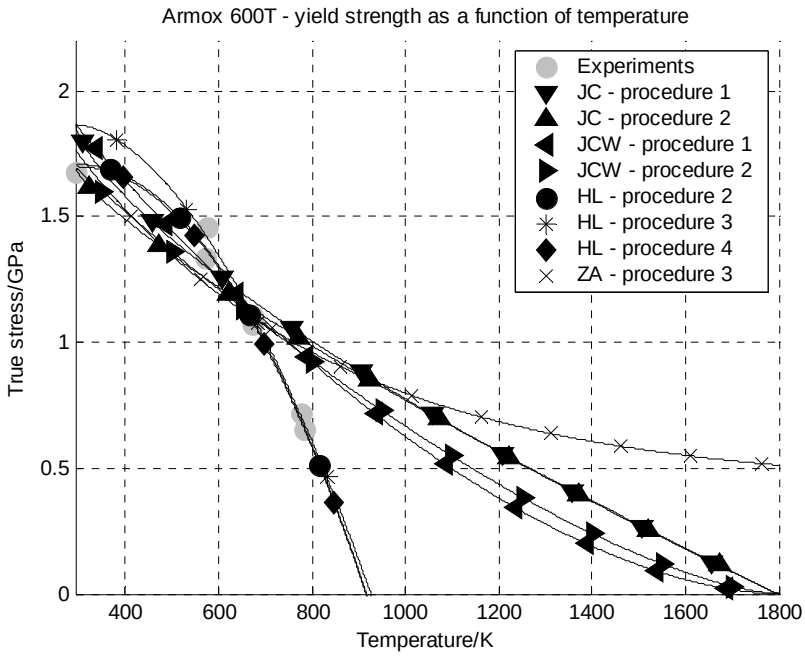

Figure 53. Yield strength at 0.1% strain, a strain rate of 1 /s and various temperatures.

It is evident that the Huang & Liang model captures the thermal softening of the material better than the other models but with the Huang & Liang model, the material will loose all strength already at about 900 K, i.e. 630 °C. On the other hand, using Zerilli & Armstrong, the strength at melting temperature, 1800 K, is still 500 MPa, but the Zerilli & Armstrong is only valid at temperatures lower than $0.5T_m$ [7].

The temperature raise under adiabatic conditions and a strain rate of 1000 /s are plotted in Figure 54 and Figure 55. As can be seen, the temperatures are about 750 K, far from the melting temperature at a plastic strain of 1.

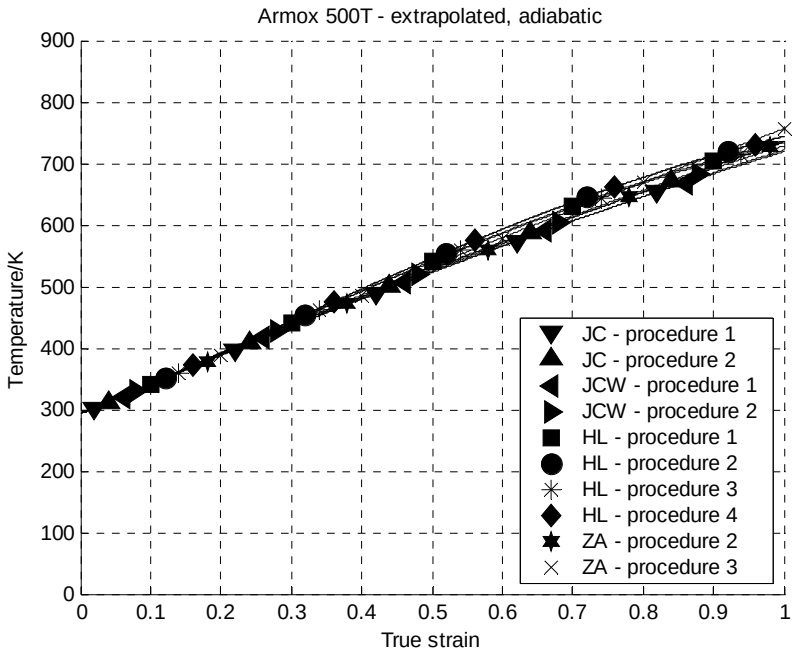

Figure 54. Adiabatic temperature increase in Armox 500T at 1000 /s.

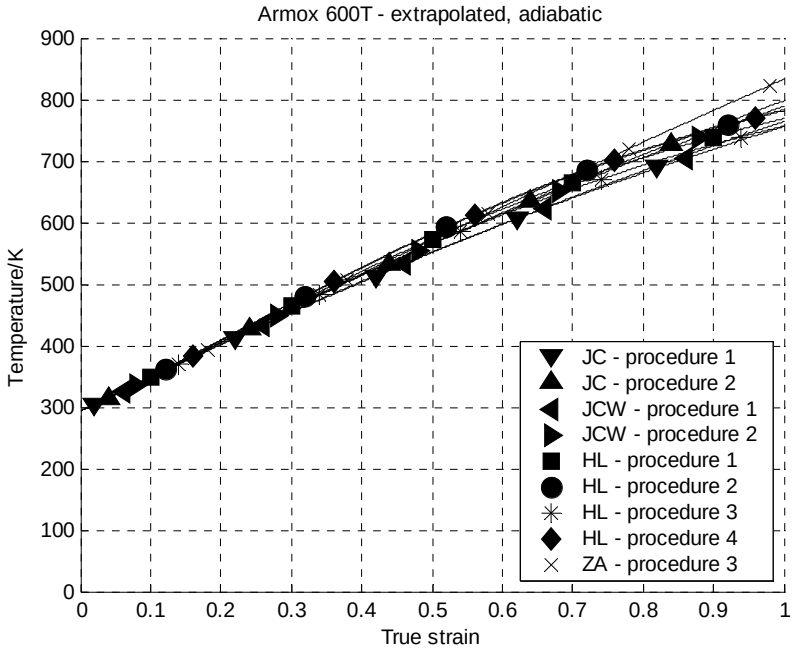

Figure 55. Adiabatic temperature increase in Armox 600T at 1000 /s.

Taking this into account, the thermal softening in the Johnson & Cook and Weerasooriya strength models seems superior, almost linearly reducing the strength with raising temperature and giving zero strength at melting temperature.

Lach et al. [17] carried out mechanical testing on a martensitic armour steel, with the German

designation 1.6568, with a hardness of 500 HV30 and compared it with work hardened nitrogen alloyed steel with a hardness of 380 HV30. For the martensitic armour steel, in compression, the yield stress reaches approximately 2.2 GPa at a true strain of 60%, and the yield stress show no strain rate hardening. Nahme and Lach [18] studied the French Mars armour steels, engineering properties are found in Table 25. The experiments show little strain rate hardening effect at strain rates up to 2500 /s. Plate impact experiments, at much higher strain rates, show a pronounced increase in strength, Table 26.

Table 25. Properties of Mars armour steels [23].

Type	**Description**	**Hardness/BH30**	$R_{P0.2}$ **/ GPa**	R_m **/ GPa**
Mars 240	High strength armour steel	470-540	1.350	1.725
Mars 300	Very high strength armour steel	>575	1.450	2.250

Table 26. Dynamic material properties of Mars armour steels from plate impact experiments [23].

Type	**Hugoniot elastic limit/ GPa**	**Spall strength (** v_0 **<700 m/s)/ GPa**	**Spall strength (** v_0 **>700 m/s)/ GPa**
Mars 240	1.2	5.9	3.4
Mars 300	1.6-2.2	5.7-6.2	---

The only results from Lach et al. [17] and Nahme and Lach [18] that can be compared with the present results are the strain rate hardening. Both the their results [17, 18] and the present results show a similar very low strain rate hardening effect compared to, for example nitrogen-alloyed steel (HNS) [3], Figure 56.

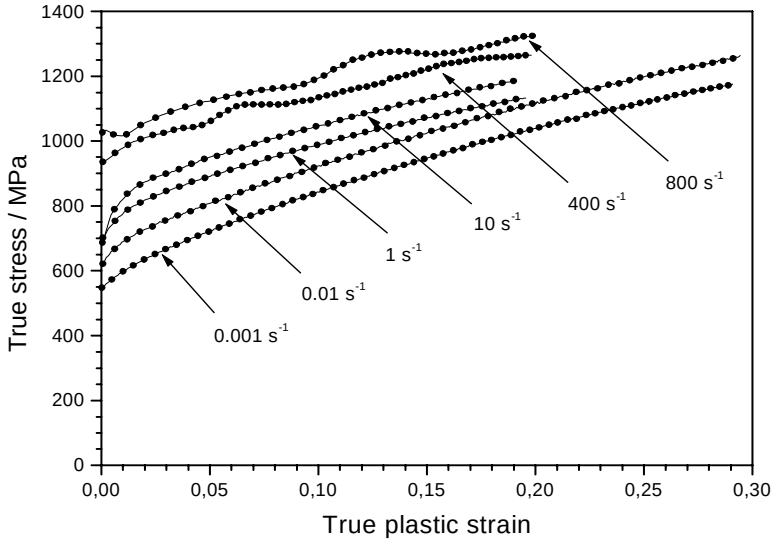

Figure 56. Strain rate hardening of HNS [3].

7 Conclusions

- Fitting experimental data to different strength models or using different fitting approaches to extract the parameters will give significantly different results when applying the extracted model to calculate the yield strength at high strain and high strain-rates.

- The main difference between the different models is the ability to capture the thermal softening.

- Armox 500T and Armox 600T shown low strain rate hardening at strain rates below 1000 /s.

8 Future work

Work is under way to extract the parameters for fracture models for Armox 500T. Experiments have been conducted with specimens with various notch dimensions to extract the pressure dependence of the fracture strain.

The strength models need to be evaluated using simulations of relatively simple events such as tensile tests or, at higher strain rates, symmetric Taylor tests. Symmetric Taylor tests have the great advantage of subjecting the sample material to high strains and strain-rates without fracture. To conduct this test a cylindrical rod of the material tested is propelled against a static rod of the same material and dimensions. The test is filmed with high-speed cameras and strain gauges can be glued to the sample to provide additional information about the strain at various points. Numeric simulations can then be compared to the silhouettes from the film and strain gauge data.

9 References

[1] G. R. Johnson and W. H. Cook, “A constitutive model and data for metals subjected to large strains, high strain rates and high temperatures” presented at 7th International Symposium on Ballistics, The Hague, The Netherlands, 1983.

[2] S. J. Savage, P. Skoglund, J. Eriksson, L.-G. Olsson and P. Persson, “Ballistic and High Strain Rate Properties of High Nitrogen Steel Compared to RHA” presented at 18th International Symposium on Ballistics, San Antonio, Texas, USA, 1999.

[3] H. Hansson and P. Skoglund, “Modeling of steel behavior with application to armor penetration”, FOI, Stockholm, (Teknisk rapport/Technical report), FOI-R--0201--SE, 2001.

[4] P. Skoglund and S. J. Savage, “Constitutive modelling and mechanical properties of a nitrogen alloyed steel”, *Journal de Physique IV Pr. 9 (DYMAT 2000)*, Vol. 10, p. 701-706, 2000.

[5] T. Weerasooriya, “Modeling flow behavior of 93W-5Ni-2Fe tungsten heavy alloy” presented at High-Pressure Science and Technology, Colorado springs, Colorado, USA, 1993.

[6] Y. Huang and S. Y. Liang, “Cutting forces modeling considering the effect of tool thermal property--application to CBN hard turning”, *International Journal of Machine Tools and Manufacture*, Vol. 43, p. 307-315, 2003.

[7] F. J. Zerilli and R. W. Armstrong, “Dislocation-mechanics based constitutive relations for materials dynamics calculations”, *Journal of Applied Physics*, Vol. 61, p. 1816, 1987.

[8] C. Albertini and M. Montagnani, “Testing techniques based on the split Hopkinson bar”, *Institute of Physics Conference Series*, Vol. 21, p. 22-32, 1974.

[9] U. S. Lindholm, “Some experiments with the split Hopkinson pressure bar”, *Journal of the Mechanics and Physics of Solids*, Vol. 12, p. 317-335, 1964.

[10] K. Kawata, S. Hashmimoto, K. Kurokawa and N. Kanayama, “A new testing method for the characterisation of materials in high-velocity tension”, *Institute of Physics Conference Series*, Vol. 47, p. 71-80, 1980.

[11] S. Ellwood, L. J. Griffiths and D. J. Parry, “A tensile technique for materials testing at high strain rates”, *Journal of Physics E-Scientific Instruments*, Vol. 15, p. 1169-1172, 1982.

[12] J. Harding and L. M. Welsh, “A tensile testing technique for fibre-reinforced composites at impact rates of strain”, *Journal of Materials Science & Technology*, Vol. 18, p. 1810-1826, 1983.

[13] T. Svensson, “Pendeldragprovare. Mäter materials ryckhållfasthet.”, FOA, Stockholm, FOA C 20577-D4, 1985.

[14] G. H. Staab and A. Gilat, “A direct-tension split Hopkinson bar for high strain-rate testing”, *Experimental Mechanics*, Vol. 31, p. 232-235, 1991.

[15] J. Erikson, A. Pettersson, M. Nilsson and P. Skoglund, “Vrid-Hopkinson - en metod för snabba skjuvbelastningar”, FOA, Stockholm, (Metodrapport/Methodology report), FOA-R--00-01775-310--SE, 2001.

[16] M. Nilsson, “Draghopkinson - en litteraturstudie”, FOA, Stockholm, (Metodrapport/Methodology report), FOA-R--00-01802-310--SE, 2000.

[17] E. Lach, G. Koerber, M. Scharf and A. Bohmann, “Comparison of nitrogen alloyed austenitic steels and high strength armor steels impacted at high velocity”, *International Journal of Impact Engineering*, Vol. 23, p. 509-517, 1999.

[18] H. Nahme and E. Lach, “Dynamic behavior of high strength armor steels”, *Journal de Physique IV, Colloque C3 (EURODYMAT 97)*, Vol. 7, p. 373-378, 1997.

[19] P. Skoglund, “Constitutive modelling and mechanical properties of a tungsten heavy metal alloy”, FOI, Stockholm, (Vetenskaplig rapport/Scientific report), FOI-R--0723--SE, 2003.

[20] P. W. Bridgman, *Studies in large plastic flow and fracture*, 2 ed., Cambridge, MA: Harvard University Press, 1964.

[21] M. A. Meyers, *Dynamic Behavior of Materials*, New York: Wiley Interscience, 1994.

[22] G. Le Roy, J. D. Embury, G. Edwards and M. F. Ashby, “A model of ductile fracture based on the nucleation and growth of voids”, *Acta Metallurgica*, Vol. 29, p. 1509-1522, 1981.

[23] H. Nahme and E. Lach, “Determination of the mechanical behavior of nitrogen alloyed steels at strain rates 10^3 $s^{-1}<d\varepsilon/dt<2\cdot10^6$ s^{-1}”, *Journal de Physique IV Pr. 9 (DYMAT 2000)*, Vol. 10, p. 287-292, 2000.

Appendix A: Experiments

Table 27. Experiments, Armox 500T.

No.	∅/mm	*l*/mm	⊥ or // to rolling direction	Equipment	Engineering strain rate/s^{-1}	T/^{o}C
A5_01	2.030	8	⊥	Single bar Hopkinson	400	20
A5_02	2.030	8	⊥	Single bar Hopkinson	400	20
A5_03	2.000	4	⊥	Single bar Hopkinson	800	20
A5_04	2.020	4	⊥	Single bar Hopkinson	800	20
A5_05*	2.020	8	⊥	MTS	0.001	20
A5_06*	2.020	8	⊥	MTS	0.001	20
A5_07	2.030	8	⊥	MTS	1	20
A5_08	1.985	8	⊥	MTS	1	400
A5_09	1.920	8	⊥	MTS	1	312
A5_11*	2.010	8	⊥	MTS	0.001	20
A5_12	2.000	8	⊥	MTS	1	510
A5_14	2.030	8	//	MTS	1	20
A5_15	2.030	8	⊥	MTS	1	315
A5_16	2.020	8	⊥	MTS	1	400
A5_17	2.020	8	⊥	MTS	1	512
A5_18	2.030	8	//	MTS	1	20

*Photographed

Table 28. Experiments, Armox 600T.

No.	∅/mm	*l*/mm	⊥ or // to rolling direction	Equipment	Engineering strain rate/s^{-1}	T/^{o}C
A6_01	2.020	8	⊥	Single bar Hopkinson	400	20
A6_02	2.010	8	⊥	Single bar Hopkinson	400	20
A6_03	1.990	4	⊥	Single bar Hopkinson	800	20
A6_04	1.990	4	⊥	Single bar Hopkinson	800	20
A6_05*	2.010	8	⊥	MTS	0.001	20
A6_06*	2.020	8	⊥	MTS	0.001	20
A6_07	1.995	8	⊥	MTS	1	20
A6_08	1.980	8	⊥	MTS	1	400
A6_09	1.995	8	⊥	MTS	1	302
A6_10	1.990	8	⊥	MTS	1	504
A6_11*	2.020	8	⊥	MTS	0.001	20
A6_13	2.030	8	//	MTS	1	20
A6_14	1.980	8	⊥	MTS	1	300
A6_15	2.020	8	⊥	MTS	1	400
A6_16	2.020	8	⊥	MTS	1	510
A6_17	2.030	8	//	MTS	1	20

*Photographed

Issuing organization	Report number, ISRN	Report type
FOI – Swedish Defence Research Agency Weapons and Protection SE-147 25 Tumba	FOI-R--1068--SE	Technical report
	Research area code 5. Combat	
	Month year December 2003	**Project no.** E2011
	Customers code 5. Commissioned Research	
	Sub area code 53 Protection and Fortification	

Author/s (editor/s)	Project manager
Martin Nilsson	Johan Magnusson
	Approved by
	Sponsoring agency Swedish Armed Forces
	Scientifically and technically responsible

Report title

Constitutive Model for Armox 500T and Armox 600T at Low and Medium Strain Rates

Abstract (not more than 200 words)

High-hardness armour steels provide a high-performance protection at a relatively low cost and is an interesting material for movable shelters. Material testing is important both because of the need for understanding the dynamic material behaviour and as input in numerical simulations of ballistic events. In this report, experiments conducted on Armox 500T and 600T, two high hardness armour steels manufactured by SSAB in Oxelösund, Sweden. The experiments have been conducted at various strain rates and temperatures and the parameters in the strength models according to Johnson & Cook and variants of the Johnson & Cook proposed by Weerasooriya and Huang and Liang respectively, and Zerilli & Armstrong have been fitted to the experimental data. To be able to include data collected after necking, the neck was photographed during the test and stress and strain corrected according to Bridgman. Experiments were conducted to test the isotropy of the steel and quasi-static yield stress and rupture strength. The experimental data was fitted to the dynamic strength models following different fitting procedures. The different procedures give different results and these are compared and checked for unphysical behaviour. Plotting the results of all strength models and procedures show that the differences between different strength models and procedures are significant. The results from the experiments are to some extent compared with data found in the literature. Both the experiments and the literature shows that high-hardness martensitic armour steels have low strain-rate hardening at medium strain-rates, $\dot{\varepsilon} < 1000$ /s , compared to for example nitrogen alloyed steel.

Keywords

armour steel, constitutive model, Johnson&Cook, Zerilli&Armstrong

Further bibliographic information	Language English
ISSN 1650-1942	**Pages** 76 p.
	Price acc. to pricelist

Utgivare	Rapportnummer, ISRN	Klassificering
Totalförsvarets Forskningsinstitut - FOI Vapen och skydd 147 25 Tumba	FOI-R--1068--SE	Teknisk rapport
	Forskningsområde 5. Bekämpning	
	Månad, år December 2003	**Projektnummer** E2011
	Verksamhetsgren 5. Uppdragsfinansierad verksamhet	
	Delområde 53 Skydd och anläggningsteknik	

Författare/redaktör	Projektledare
Martin Nilsson	Johan Magnusson
	Godkänd av
	Uppdragsgivare/kundbeteckning Försvarsmakten
	Tekniskt och/eller vetenskapligt ansvarig

Rapportens titel (i översättning)

Konstitutiv modell för Armox 500T och Armox 600T vid låga och medelhöga töjningshastigheter

Sammanfattning (högst 200 ord)

Höghållfasta pansarstål ger en hög nivå av skydd mot vapenverkan till en relativt låg kostnad och är ett intressant material för flyttbara skydd. Materialprovning är viktig både för att öka förståelsen om dynamiskt materialbeteende och för att kunna göra numeriska simuleringar av ballistiska förlopp. I den här rapporten presenteras försök utförda på Armox 500T och 600T, två höghållfasta pansarstål tillverkade av SSAB i Oxelösund, Sverige. Försöken har utförts vid olika töjningshastigheter och temperaturer och sedan har parametrarna i spänningsmodellen Johnson & Cook och två varianter av Johnson & Cook, föreslagna av Weerasooriya respektive Huang and Liang, och Zerilli & Armstrongs modell anpassats till experimentella data. För att kunna använda data insamlade efter att lokaliserad töjning uppträtt i provstavarna fotograferades proven under provförloppet och spänning och töjning korrigerades enligt den av Bridgman föreslagna korrektionen. Försök utfördes för att undersöka isotropin hos stålen och för att fastställa kvasistatisk flytspänning och brottspänning. Experimentella data anpassades till de olika modellerna enligt olika rutiner. De olika rutinerna gav olika resultat och dessa jämfördes och kontrollerades för att upptäcka ofysikaliskt beteende. När resultaten jämfördes visade sig påtagliga skillnader mellan modeller och rutiner. Resultaten från försöken jämförs med data i litteraturen. Både försöken och litteraturdata visar att höghållfasta martensitiska pansarstål har lågt töjningshastighetshårdnande vid medelhöga töjningshastigheter, $\dot{\varepsilon} < 1000$ /s , jämfört med exempelvis kvävelegerat stål.

Nyckelord

pansarstål, konstitutiv modell, Johnson&Cook, Zerilli&Armstrong

Övriga bibliografiska uppgifter	Språk Engelska
ISSN 1650-1942	**Antal sidor:** 76 s.
Distribution enligt missiv	**Pris: Enligt prislista**